DE-NOISING MEMS VIBRATING GYRO USING WAVELET TRANSFORM

A Thesis

submitted towards the partial fulfillment of

the requirements of the degree of

Master of Engineering

in

Electronics Instrumentation and Control Engineering

submitted by

Sangram Keshari Das

Roll No- 800851017

under the supervision of

Dr. Yaduvir Singh

Associate Professor (EIED)

and

Dr. Hardeep Singh

Assistant Professor (ECED)

DEPARTMENT OF ELECTRICAL AND INSTRUMENTATION ENGINEERING

THAPAR UNIVERSITY

PATIALA – 147004

JULY-2010

CERTIFICATE

This is to certify that my work presented in this thesis entitled ***"De-Noising MEMS Vibrating Gyro Using Wavelet Transform"*** *submitted in partial fulfillment of the requirement for the award of the degree of* ***Master of Engineering in Electronics Instrumentation and Control Engineering at Thapar University, Patiala****, is an original record under supervision and guidance of* ***Dr. Yaduvir Singh*** (Associate Professor, EIED) and Dr. ***Hardeep Singh*** (Assistant Professor, ECED) *.The matter embodied in this report has not been submitted anywhere for the award of any degree.*

Date: 06.07.2010

SANGRAM KESHARI DAS

ROLL NO-800851017

It is certified that the above statement made by the student is correct to the best of our knowledge and belief.

Dr.Yaduvir Singh

Associate Professor, EIED

Thapar university, Patiala

Dr. Hardeep Singh

Assistant Professor, ECED

Thapar university, Patiala

Dr. Smarajit Ghosh

Professor & Head EIED

Thapar University, Patiala

Dr. R.K.Sharma

Dean of Academic Affairs

Thapar University, Patiala

Dedicated to my Parents

Shri. P.C.DAS

&

Smt. Bharati Das

Acknowledgment

The real spirit of achieving a goal is through the way of excellence and austere discipline. I would have never succeeded in completing my task without the co-operation, encouragement and help provided to me by various personalities.

With deep sense of gratitude I express my sincere thanks to my esteemed and worthy Supervisor, **Dr. Yaduvir Singh**, Associate Professor, Department of Electrical & Instrumentation Engineering, Thapar University, Patiala, for his valuable guidance in carrying out this work under his effective supervision, encouragement, enlightenment and co-operation.

I shall be failing in my duties if I do not express my deep sense of Gratitude towards Dr. Smarajit Ghosh, Professor & Head of the Department of Electrical & instrumentation Engineering, Thapar University, Patiala who has been a constant source of inspiration for me throughout this work.

I am also thankful to all the staff members of the Department for their full co-operation and help.

This acknowledgement would be incomplete if I do not mention the emotional support and blessings provided by my friends. I had a pleasant enjoyable and fruitful company with them.

My greatest thanks are to all who wished me success especially my parents, my brother and sister. Above all I render my gratitude to **The ALMIGHTY** who bestowed self-confidence, ability and strength in me to complete this thesis work.

DATE: **SANGRAM KESHARI DAS**

PLACE

ABSTRACT:

In this thesis report, the theory of MEMS vibratory gyroscope is introduced and discrete wavelet decomposition and reconstruction are introduced. In the first part of this work, I review the Coriolis effect and angular rate sensors, and fundamental operational principles of micro-machined vibratory gyroscopes. The MEMS gyroscopes are expected to lead to reliable, robust and high performance angular-rate sensors with low production costs and high yields, fitting into or enabling many applications in the aerospace/defense, automotive and consumer electronics markets.

Then the method of de-noising of the noised signal using wavelet decomposition and thresholding method are described. Noise estimation, threshold selection methods are also given. The specifications of the Rate Sensor Gyro – RRS01-03-0100 are given in the third chapter.

At last, the experimental results are discussed. The experimental results show that the method presented can greatly reduce the noise in the gyro's output signal and improve the performance of the system.

In this work , the data analysis approach to be described can be understood as a transform which maps a hierarchical clustering into a transformed set of data; and this transform is invertible, meaning that the original data can be exactly reconstructed. Such transforms are very often used in data analysis and signal processing because processing of the data may be facilitated by carrying out such processing in transform space, followed by reconstruction of the data in some "good approximation" sense.

TABLE OF CONTENTS:

LIST OF FIGURE:

List of Table :

Literature survey:

V. Herrero et al. in their paper [1] gives basic ideas of Wavelet Transform which has shown itself as an useful tool in the field of 1-D and 2-D signal compression systems. Due to the growing importance of this technique, there was an increasing need in many working groups for having a development environment which could be flexible enough and where the performance of a specific architecture could be measured, closer to reality rather than in a theoretical way.

Ranran Yi et al. in their paper [2] have analysed the closed-loop circuit of MEMS gyroscope from two aspects of amplitude fixed and frequency locking. Different levels of simulation and circuit implementation are made using the working mode and parameter of the dual-tuner output-quality pieces of silicon MEMS gyroscope which is designed by their own laboratory.

Woon-Tahk Sung et al. in their paper [3] have discussed " the development and performance test results of a laterally oscillating MEMS gyroscope" using a novel force rebalance control strategy. The micromachined structure and electrodes are fabricated using the deep reactive ion etching (DRIE) and anodic wafer bonding process. The high quality factor required for the resonance-based sensor is achieved using a vacuum-sealed device package. A systematic design approach of the force rebalance control is applied via a modified automatic gain control (AGC) method.

Steven Nasiri in his paper [4] has presented Gyroscopes which are expected to become the next "killer" application for the MEMS industry in the coming years. A multitude of applications already have been developed for consumer and automotive markets. Some of the more well known automotive applications such as vehicle stability control, navigation assist, roll over detection are only used in high-end cars, where cost is not a

major factor. Advancement in MEMS technology, fueled by the optical bubble, such as, wafer-scale-integration, and wafer-scale-packaging will be reviewed. New opportunities for design and development of the next generation of low-cost and high-performance gyroscopes based on the latest MEMS technologies are discussed.

Wang Chang-hong In his paper [7] , has introduced the theory of wavelet packet analysis and the algorithms of wavelet packet decomposition and reconstruction. Then, the method of the application of wavelet packet analysis in the de-nosing of a MEMS vibrating ring gyro is given. *At* last, the effectiveness of this method is verified by an experiment. Noise introduces certain uncertainty into the measurement that de-generates the gyroscopic performances.

Fuqiang Liu et al. in their paper [8] ananlysed the MEMS gyro's output signal's error characteristic fist. Then, on the basis of the principle study of Wavelet Analysis Methods, a wavelet denoising technique is implied to the gyro output signal and examined by the practical experiments in order to specify appropriate wavelet function and according parameters both for static and dynamic state. The experiment results show that the method presented can greatly reduce the noise in the gyro's output signal and improve dynamic performance of the system.

Robi Polikar in his tutorial paper [12] has described about the introductory tutorial on wavelet transforms. In his tutorial he has presented basic principles underlying the wavelet theory. Most of the signals in practice, are TIME-DOMAIN signals in their raw format. That is, whatever that signal is measuring, is a function of time. In other words, when we plot the signal one of the axes is time (independent variable), and the other (dependent variable) is usually the amplitude. When we plot time-domain signals, we obtain a time-amplitude representation of the signal. This representation is not always the best representation of the signal for most signal processing related applications.

JICHANG GUO et al. in their paper [15] described about the relationship between stationary and classic wavelet is studied in detail. For the first time, the stationary wavelet is used to the de-noising of gyro signals. The de-noising result is compared with that of classic wavelet. It shows that the north finding accuracy by using stationary wavelet is obviously better than that by using classic wavelet. It also proves the better de-noising performance of stationary wavelet.

Isaac Skog in his paper [16] approach for calibrating a low-cost IMU is studied, requiring no mechanical platform for the accelerometer calibration and only a simple rotating table for the gyro calibration. The proposed calibration methods utilize the fact that ideally the norm of the measured output of the accelerometer and gyro cluster are equal to the magnitude of applied force and rotational velocity, respectively. This fact, together with model of the sensors is used to construct a cost function, which is minimized with respect to the unknown model parameters using Newton's method. The performance of the calibration algorithm is compared with the Cram´er-Rao bound for the case when a mechanical platform is used to rotate the IMU into different precisely controlled orientations. Simulation results shows that the mean square error of the estimated sensor model parameters reaches the Cram´er-Rao bound within 8 dB, and thus the proposed method may be acceptable for a wide range of low-cost applications.

Gaoyou Tian et al. in their paper [17] discussed the application of wavelet denoising (WD) to near infrared derivative spectra was investigated. The parameters such as wavelet function, threshold calculation and scale level were studied in detail. The WD performance was evaluated by means of ratio of signal-noise (S/N) and the predictive ability for RON (Research Octane Number) of gasoline. The results show that wavelet function and scale level have great effects on WD performance. WD can reduce markedly the noise from near infrared derivative spectra; improve effectively S/N and RON analysis accuracy. WD methods were compared with Fourier Transform denoising (FTD) and S-G smoothing (SGS) respectively. Wavelet methods are better than others.

Huikai Xie et al. in their paper [21] reviewed Micro-electromechanical MEMS gyroscopes have wide-ranging applications including automotive and consumer electronics markets. Among them, complementary metal-oxide semiconductor-compatible MEMS gyroscopes enable integration of signal conditioning circuitry, multiaxis integration, small size, and low cost. This paper reviews various designs and fabrication processes for integrated MEMS gyroscopes and compares their performance. Operational principles and design issues of MEMS vibratory gyroscopes are also addressed.

CHAPTER 1

Fundamentals of MEMS Gyroscopes :

In this chapter, MEMS Technology and the fundamental operational principles of micro-machined vibratory rate gyroscopes have been reviewed. First, the dynamics of linear and torsional vibratory gyroscope sensing elements are developed. Then, oscillation patterns and the characteristics of the gyroscope response to the rotation-induced Coriolis force are analyzed, considering basic phase relations and oscillation patterns.

1.0 The MEMS Technology:

As the name implies, Micro-electromechanical Systems (MEMS) is the technology that combines electrical and mechanical systems at a micro scale. Practically, any device fabricated using photo-lithography based techniques with micrometer (1mm =10¯6m) scale features that utilizes both electrical and mechanical functions could be considered MEMS.

Evolved from the semiconductor fabrication technologies, the most striking feature of the MEMS technology is that it allows building moving micro-structures on a substrate. With this capability, extremely complex mechanical and electrical systems\ can be created. Masses, flexures, actuators, detectors, levers, linkages, gears, dampers, and many other functional building blocks can be combined to build complete sophisticated systems on a chip. Inertial sensors such as accelerometers and gyroscopes utilize this capability to its fullest.

Photolithography based pattern transfer methods and successive patterning of thin structural layers adapted from standard IC fabrication processes are the enabling technologies behind micromachining. By dramatically miniaturizing and batch processing complete electro-mechanical systems, substantial reductions in device size, weight and cost are achieved.

1.1 **Dynamics of Vibratory Rate Gyroscopes**

The basic architecture of a vibratory gyroscope is comprised of a drive-mode oscillator that generates and maintains a constant linear or angular momentum, coupled to a sense-mode Coriolis accelerometer that measures the sinusoidal Coriolis force induced due to the combination of the drive vibration and an angular rate input.

The vast majority of reported micro-machined rate gyroscopes utilizes a vibratory proof mass suspended by flexible beams above a substrate. The primary objective of the dynamical system is to form a vibratory drive oscillator, coupled to an orthogonal sense accelerometer by the Coriolis force. Both the drive-mode oscillator and the sense-mode accelerometer can be implemented as either linear or torsional resonators. In the case of a linear vibratory gyroscope, a Coriolis force is induced due to linear drive oscillations, while in a torsional vibratory gyroscope, a Coriolis torque is induced due to rotary drive oscillations.

A type of MEMS gyroscope uses a vibrating element to sense angular rate through the detection of Coriolis acceleration. The vibrating element is put into oscillatory motion in the X-axis (drive plane), which is parallel to the substrate. Once the vibrating element is put in motion, it is capable of detecting angular rates induced by the substrate being rotated about the Z-axis (input plane), which is perpendicular to the substrate. The Coriolis acceleration occurs in the Y-axis (sense plane), which is orthogonal to both the X-axis and the Z-axis. The Coriolis acceleration produces a Coriolis motion that has amplitude and that is proportional to the angular rate of the substrate. An excited vibration mode (primary mode) is coupled into sense mode (secondary mode) due to the

Coriolis acceleration when there is an input angular velocity. The magnitude of oscillation in the sense mode provides a measure of the input angular velocity. This type of gyros has a lot of advantages compared to the Spinning Mass Gyroscope and Optical Gyroscope such as requiring no rotational parts, suitable for mass production and almost free of maintenance. So it has been used in many applications. But its output signal contains noise. Noise introduces certain uncertainty into the measurement, which degenerate the gyroscopic performances. So elimination of the noise is very important in the gyro output signal processing.

The output signal of gyro is non-stationary. So, Fourier analysis is not effective to de-noise the signal. Wavelet based de-noising techniques are effective due to its compression of information signal and incompressibility of noise signal [5]. In wavelet based de-noising, a threshold is determined and a wavelet coefficient should be preserved or eliminated on the basis on threshold. Donoho and Johnstone [6] developed class of simple and effective de-noising methods by introducing a threshold on wavelet coefficient. Wang Chang- Hong and Huang Xu [7] introduced wavelet packet for de-noising out put signal of a Gyro. F. Lue et al. [8] used threshold based wavelet filter to de-noise the gyro's output signal.

1.1.1 Linear Gyroscope Dynamics

The most basic implementation for a micro-machined vibratory rate gyroscope is a single proof mass suspended above the substrate. The proof mass is supported by anchored flexures, which serve as the flexible suspension between the proof mass and the substrate, making the mass free to oscillate in two orthogonal directions - the drive and the sense directions (Figure 1.1).

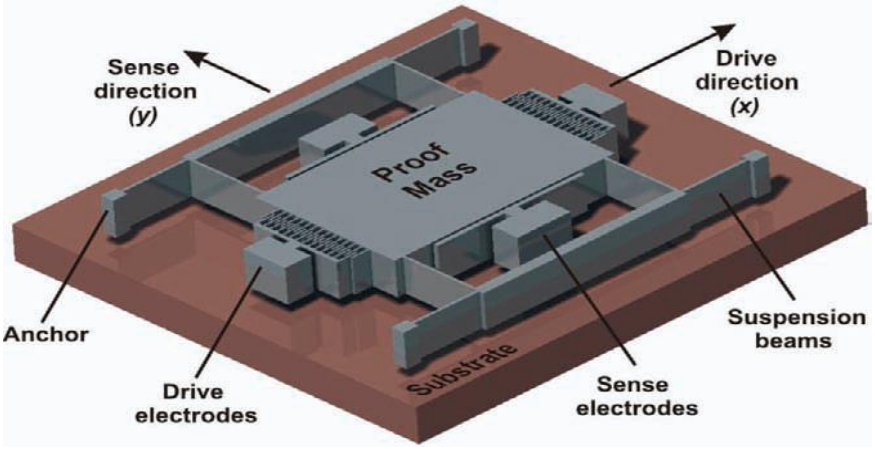

FIG. 1.1 A generic MEMS implementation of a linear vibratory rate gyroscope.

A proof-mass is suspended above a substrate using a suspension system comprised of flexible beams, anchored to the substrate. One set of electrodes is needed to excite the drive-mode oscillator, and another set of electrodes detects the sense-mode response. The drive-mode oscillator is comprised of the proof-mass, the suspension system that allows the proof-mass to oscillate in the drive direction, and the drive-mode actuation and feedback electrodes. The proof-mass is driven into resonance in the drive direction by an external sinusoidal force at the drive-mode resonant frequency. The sense-mode accelerometer is formed by the proof-mass, the suspension system that allows the proof-mass to oscillate in the sense direction, and the sense-mode detection electrodes. When the gyroscope is subjected to an angular rotation, a sinusoidal Coriolis force at the frequency of drive-mode oscillation is induced in the sense direction. The Coriolis force excites the sense-mode accelerometer, causing the proof-mass to respond in the sense direction. This sinusoidal Coriolis response is picked up by the detection electrodes.

For a generic z-Axis gyroscope, the proof mass is required to be free to oscillate in two orthogonal directions: the drive direction (x-Axis) to form the vibratory oscillator, and the sense direction (y-Axis) to form the Coriolis accelerometer. The overall dynamical system becomes simply a two degrees-of-freedom (2-DOF) massspring-damper system (Fig. 1.2).

The dynamics and principle of operation can be best understood by considering the rotation-induced Coriolis force acting on a body that is observed in a rotating reference

frame. One of the most intuitive methods to obtain the equations of motion is taking the second time derivative of the position vector to express the acceleration of a body moving with the rotating reference frame.

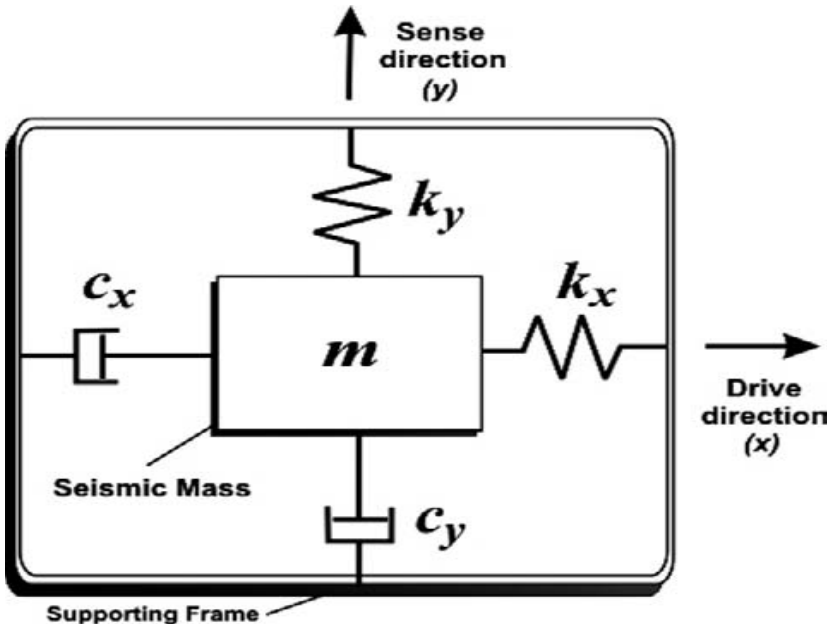

FIG. 1.2 A vibratory rate gyroscope is comprised of a proof mass which is free to oscillate in two principle orthogonal directions: drive and sense.

The accelerations experienced by a moving body in a rotating reference frame can be conveniently derived starting with the following definitions:

A : Inertial (stationary) frame

B : Non-inertial (rotating) reference frame

rA : Position vector relative to inertial frame A

rB : Position vector relative to rotating frame B

q : Orientation vector of rotating frame B relative to inertial frame A

W : Angular velocity vector of rotating frame B, $W = \dot{q}$

R : Position vector of rotating frame B

The time derivative of a vector r, which is defined in the two reference frames A and B as $\mathbf{r}_A$ and $\mathbf{r}_B$, respectively, is given as

$$\dot{\mathbf{r}}_A(t) = \dot{\mathbf{r}}_B(t) + \dot{\theta} \times \mathbf{r}_B(t) \tag{1.1}$$

Taking the second time derivative of the position vector r, the acceleration of a body moving with the rotating reference frame can be calculated as

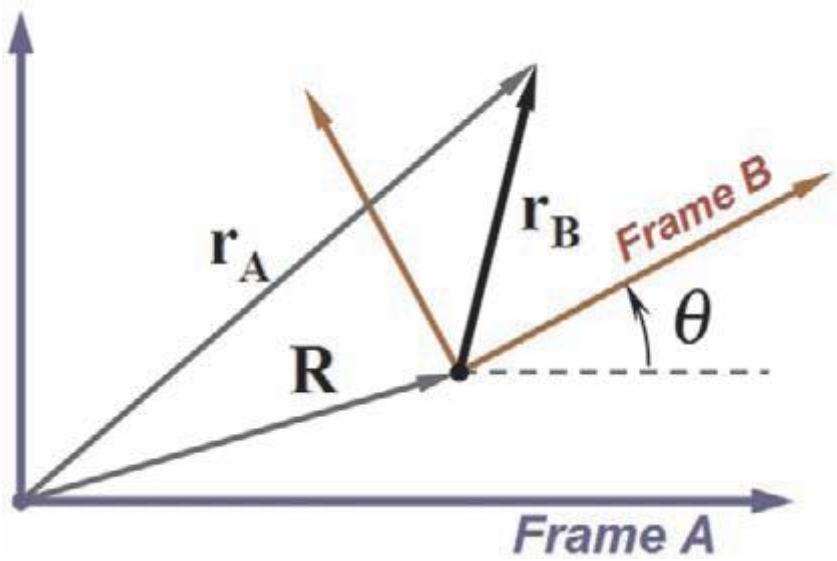

FIG. 1.3 Representation of the position vector relative to the inertial frame A and the rotating reference frame B.

$$\mathbf{r}_A(t) = \mathbf{R}(t) + \mathbf{r}_B(t) \tag{1.2}$$

$$\dot{\mathbf{r}}_A(t) = \dot{\mathbf{R}}(t) + \dot{\mathbf{r}}_B(t) + \dot{\theta} \times \mathbf{r}_B(t) \tag{1.3}$$

$$\ddot{\mathbf{r}}_A(t) = \ddot{\mathbf{R}}(t) + \ddot{\mathbf{r}}_B(t) + \dot{\theta} \times \dot{\mathbf{r}}_B(t) + \dot{\theta} \times (\dot{\theta} \times \mathbf{r}_B(t)) + \ddot{\theta} \times \mathbf{r}_B(t) + \dot{\theta} \times \dot{\mathbf{r}}_B(t) \tag{1.4}$$

With the definition of vB and aB as the velocity and acceleration vectors with respect to the rotating reference frame B, aA as the acceleration vector with respect to the inertial frame A, A as the linear acceleration of the reference frame B, and W as the angular velocity vector of the reference frame B; the expression for acceleration reduces to

$$\mathbf{a}_A = \mathbf{A} + \mathbf{a}_B + \dot{\Omega} \times \mathbf{r}_B + \Omega \times (\Omega \times \mathbf{r}_B) + 2\Omega \times \mathbf{v}_B \tag{1.5}$$

In this equation, $(\mathbf{A}+\mathbf{a_B}+\dot{\Omega}\times\mathbf{r_B})$ is the local acceleration, and $\Omega\times(\Omega\times\mathbf{r_B})$ is the centripetal acceleration. The last term $2\Omega\times\mathbf{v_B}$ is the Coriolis acceleration, which is the primary mechanism that scales and converts the rotation rate of the rotating reference frame B into a fictitious inertial force when observed in the rotating frame.

When applied to the position vector of a vibratory gyroscope proof-mass, this analysis yields the dynamics of the gyroscope attached to a rotating object. The equation of motion of the proof-mass can be derived by expressing the acceleration vector of the proof mass with respect to the inertial frame A by taking the second time derivative of the position vector (Figure 2.4),

$$\mathbf{F_{ext}} = m\left[\mathbf{A}+\mathbf{a_B}+\dot{\Omega}\times\mathbf{r_B}+\Omega\times(\Omega\times\mathbf{r_B})+2\Omega\times\mathbf{v_B}\right] \tag{1.6}$$

where A is the linear acceleration and W is the angular velocity of the rotating gyroscope frame, $\mathbf{v_B}$ and $\mathbf{a_B}$ are the velocity and acceleration vectors of the proof mass with respect to the reference frame, and **F**ext is the total external force applied on the proof mass.

In a z-Axis gyroscope, the two principle oscillation directions are the drive direction along the x-axis and the sense direction along the y-axis. Decomposing the motion into the two principle oscillation directions and assuming that the linear accelerations are negligible, the two equations of motion along the drive and sense axes can be expressed as

$$m\ddot{x}+c_x\dot{x}+(k_x-m(\Omega_y{}^2+\Omega_z{}^2))x+m(\Omega_x\Omega_y-\dot{\Omega}_z)y=\tau_x+2m\Omega_z\dot{y}$$

$$m\ddot{y}+c_y\dot{y}+(k_y-m(\Omega_x{}^2+\Omega_z{}^2))y+m(\Omega_x\Omega_y+\dot{\Omega}_z)x=\tau_y-2m\Omega_z\dot{x}$$

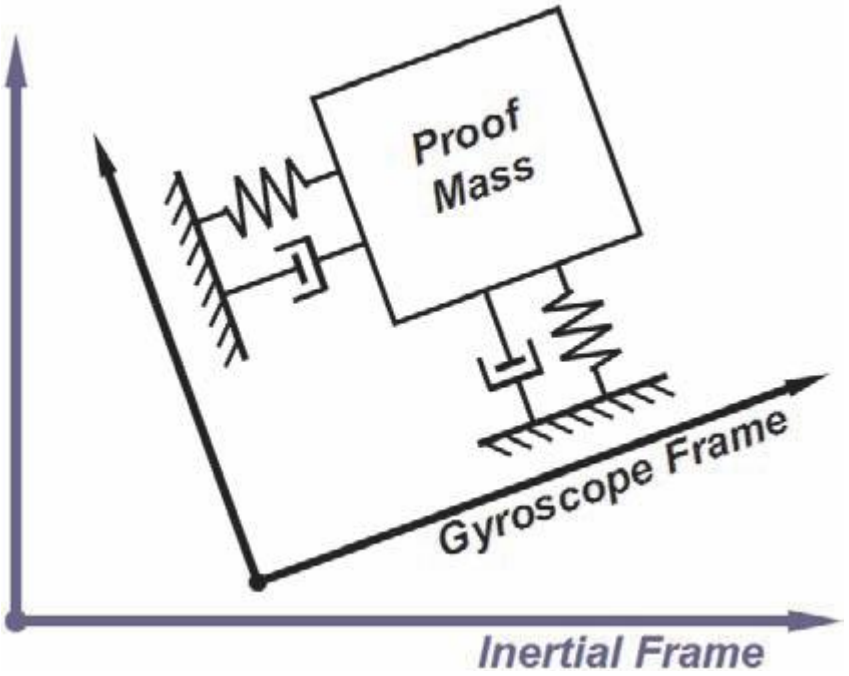

Fig. 1.4

Schematic illustration of the gyroscope frame rotating with respect to the inertial frame.

For a constant angular rate input $\dot{\Omega}_z = 0$, and for angular rates at much lower frequencies than the operating frequency of the gyroscope, the terms $\Omega_x{}^2$, $\Omega_y{}^2$, and $\Omega_x\Omega_y$ become negligible. Since the sense-mode response is usually orders of magnitude smaller in amplitude than the drive motion, the Coriolis term $2m\Omega_z\dot{y}$ is also negligible. Thus, the practical simplified 2-DOF equations of motion of a vibratory rate gyroscope become:

$$m\ddot{x} + c_x\dot{x} + k_x x = \tau_x \tag{1.7}$$

$$m\ddot{y} + c_y\dot{y} + k_y y = \tau_y - 2m\Omega_z\dot{x} \tag{1.8}$$

Where τ_x is the external force in the drive direction, which is usually a sinusoidal drive excitation force, and τ_y is the total external force in the sense direction, comprised of parasitic and external inertial forces. The term $2m\Omega_z\dot{x}$ in the sense-mode equation is the

rotation-induced Coriolis force, which causes the sense-mode response proportional to the angular rate.

A very common method to amplify the mechanical response of the sense-mode accelerometer to the Coriolis force is to design the resonant frequency of the sense-mode accelerometer close to the frequency of the Coriolis force. If the Coriolis force frequency, and thus the drive-mode resonant frequency, is matched with the sense mode resonant frequency, the Coriolis force excites the system into resonance in
the sense direction. This allows to amplify the resulting oscillation amplitude in the sense direction by the sense-mode Q factor, which could mean orders of magnitude improvement in sensitivity as explained in the following sections.

1.1.2 **Torsional Gyroscope Dynamics**

Even though conservation of both linear and angular momentum are required to express the complete dynamics of a gyroscope proof mass, linear gyroscope systems can be modeled based on conservation of linear momentum only, assuming negligible
angular deflections. Similarly, the dynamics of a torsional gyroscope can be analyzed based on conservation of angular momentum with the assumption that the linear deflections are negligible.

The angular momentum of a mass with an inertia tensor I and an angular velocity vector ω is $\mathbf{H} = \mathbf{I}\omega$. Expressing the angular momentum H in an inertial frame, angular momentum balance under the presence of an external moment M is

$$\frac{d\mathbf{H}}{dt} = \mathbf{M} \tag{1.9}$$

When the angular momentum is expressed in a non-inertial coordinate frame which rotates with the same angular velocity w as the mass, the inertia tensor I becomes constant and diagonal, and the angular momentum balance becomes

$$\mathbf{I}\dot{\omega} + \omega \times (\mathbf{I}\omega) = \mathbf{M} \tag{1.10}$$

If we consider a simple case of a z-axis torsional gyroscope with a gimbal, the dynamics of each rotary proof-mass in the torsional gyroscope system is best understood by attaching non-inertial coordinate frames to the center-of-mass of each proof-mass and the substrate (Figure 1.5). The angular momentum equation for each mass will be expressed in the coordinate frame associated with that mass. This allows the inertia matrix of each mass to be expressed in a diagonal and time-invariant form. The absolute angular velocity of each mass in the coordinate frame of that mass will be obtained using the appropriate transformations. By conservation of angular momentum, the equations of motion of the masses are

$$\mathbf{I}_s\dot{\omega}_s^s + \omega_s^s \times (\mathbf{I}_s\omega_s^s) = \tau_{se} + \tau_{sd} \tag{1.11}$$

$$\mathbf{I}_d\dot{\omega}_d^d + \omega_d^d \times (\mathbf{I}_d\omega_d^d) = \tau_{de} + \tau_{dd} + M_d \tag{1.12}$$

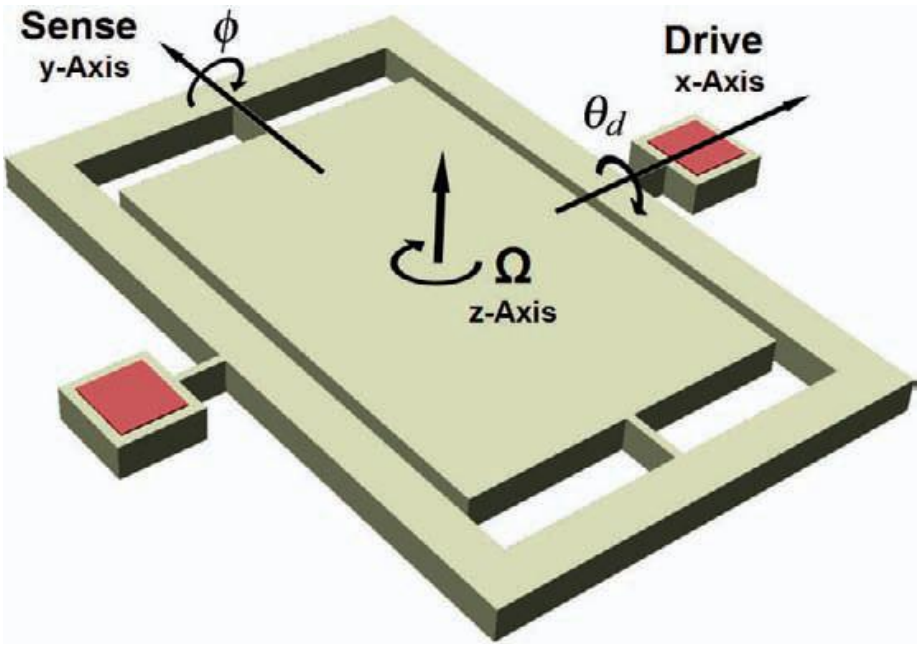

FIG.1.5 Torsional z-Axis gyroscope with drive gimbal structure. The drive-mode deflection angle of the gimbal is qd , and the sense-mode deflection angle of the sensing mass is Φ.

where Is and Id denote the diagonal and time-invariant inertia matrices of the sensing mass and the drive gimbal, respectively, with respect to the associated body attached frames. Similarly, ω_s^s and ω_d^d are the absolute angular velocity of the sensing mass and the gimbal, respectively, expressed in the associated body frames. The external torques Tse and Tde are the elastic torques, and Tsd and Tdd are the damping torques acting on the associated mass, whereas Md is the driving electrostatic torque applied to the drive gimbal. If we denote the drive direction deflection angle of the drive gimbal by θd the sense direction deflection angle of the sensing mass by f (with respect to the substrate), and the absolute angular velocity of the substrate about the z-axis by Wz as in Figure 1.5, the homogeneous rotation matrices from the substrate to drive gimbal $(R_{sub\to d})$, and from drive gimbal to the sensing mass $(R_{d\to s})$, respectively.

1.2 Resonance Characteristics

Vast majority of micromachined vibratory gyroscopes employ a combination of proof-masses and flexures to form 1 degree-of-freedom (1-DOF) resonators in both the drive and sense directions. Thus, understanding the dynamics and response characteristics of a generic 1-DOF resonator is critical in the design of both the drive and the sense-mode oscillators of a vibratory gyroscope.

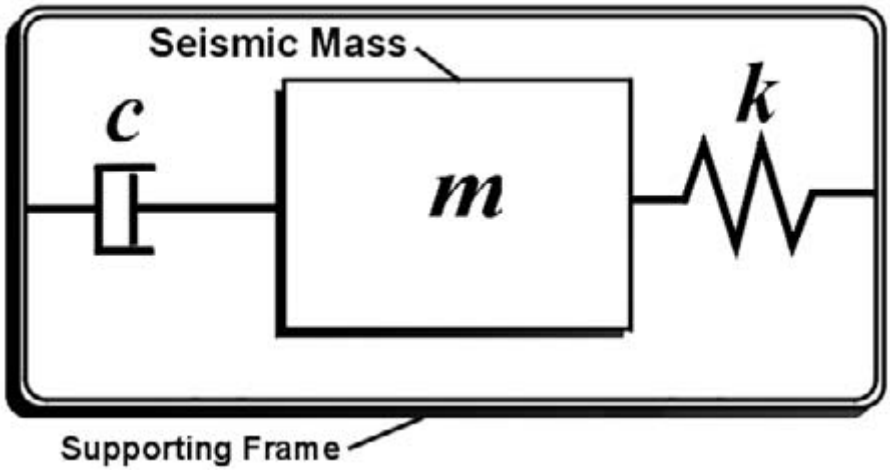

Fig. 1.6 The lumped mass-spring-damper model of a typical 1-DOF resonator.

Let us start by investigating the dynamics of a typical 1-DOF resonator as in Figure 1.6. The equation of motion of the resonator with a proof-mass m, a combined stiffness of k, and a damping factor of c is

$$m\ddot{x} + c\dot{x} + kx = F(t) \tag{1.13}$$

With the definition of the undamped natural frequency ω_n and the damping factor ξ which represents the ratio of damping to critical damping $(2\sqrt{km})$, the equation of motion becomes

$$\ddot{x} + 2\xi\omega_n\dot{x} + \omega_n^2 x = \frac{F(t)}{m} \tag{1.14}$$

$$\omega_n = \sqrt{\frac{k}{m}} \tag{1.15}$$

$$\xi = \frac{c}{c_c} = \frac{c}{2\sqrt{km}} = \frac{c}{2m\omega_n} \tag{1.16}$$

In the Laplace domain, the transfer function of the 1-DOF resonator is simply

$$\frac{X(s)}{F(s)} = \frac{\frac{1}{m}}{s^2 + 2\xi\omega_n s + \omega_n^2} \tag{1.17}$$

When the resonator is excited with a harmonic force F = Fo sinwt at the frequency w, the steady-state component of the response is also harmonic, of the form

$$x = x_0 \sin(\omega t + \phi) \tag{1.18}$$

$$x_0 = \frac{\frac{F_0}{k}}{\sqrt{\left[1 - \left(\frac{\omega}{\omega_n}\right)^2\right]^2 + \left[2\xi\frac{\omega}{\omega_n}\right]^2}}$$

(1.19)

$$\phi = -\tan^{-1}\frac{2\xi\frac{\omega}{\omega_n}}{1-\left(\frac{\omega}{\omega_n}\right)^2} \tag{1.20}$$

In the presence of considerable damping, the amplitude expression is maximized at the frequency

$$\omega_r = \omega_n\sqrt{1-2\xi^2} \tag{1.21}$$

For lightly damped systems, i.e. $\xi \ll 1$, the amplitude is maximized at the natural Frequency ω_n, and the amplitude at resonance becomes

$$|x_0|_{res} = \frac{F_0}{2k\xi} = \frac{F_0}{c\omega_n} \tag{1.22}$$

The Quality factor of the system is defined as maximum ratio of the amplitude to the static deflection, which is F0=k. Taking the ratio of the amplitude at resonance to the static deflection, the Q factor of a lightly damped system reduces to

$$Q = \frac{1}{2\xi} = \frac{m\omega_n}{c} \tag{1.23}$$

It should be noticed that the Quality factor is one of the most important parameters of a resonator, since it directly scales the amplitude at resonance. For example, for a resonator with a known Q factor, the oscillation amplitude at resonance can be found as

$$|x_0|_{res} = Q\frac{F_0}{k} \tag{1.24}$$

At the resonant frequency, the phase is -90° shifted from the forcing function phase. At frequencies lower than the resonant frequency, the phase approaches 0°, meaning that the position follows the forcing function closely. At frequencies higher than the resonant

frequency, the phase approaches -180º. The transition from 0° to -180º around the resonant frequency becomes more abrupt for higher Q values.

The bandwidth or the half-power bandwidth of the system is defined as the difference between the frequencies where the power is half of the resonance power. Since the power is proportional to the square of the oscillation amplitude, the half-power frequencies are solved by equating the amplitude expression to $1/\sqrt{2}$ times the resonance amplitude. For small values of damping, the bandwidth is approximated as

$$BW \approx \frac{\omega_n}{Q} \tag{1.25}$$

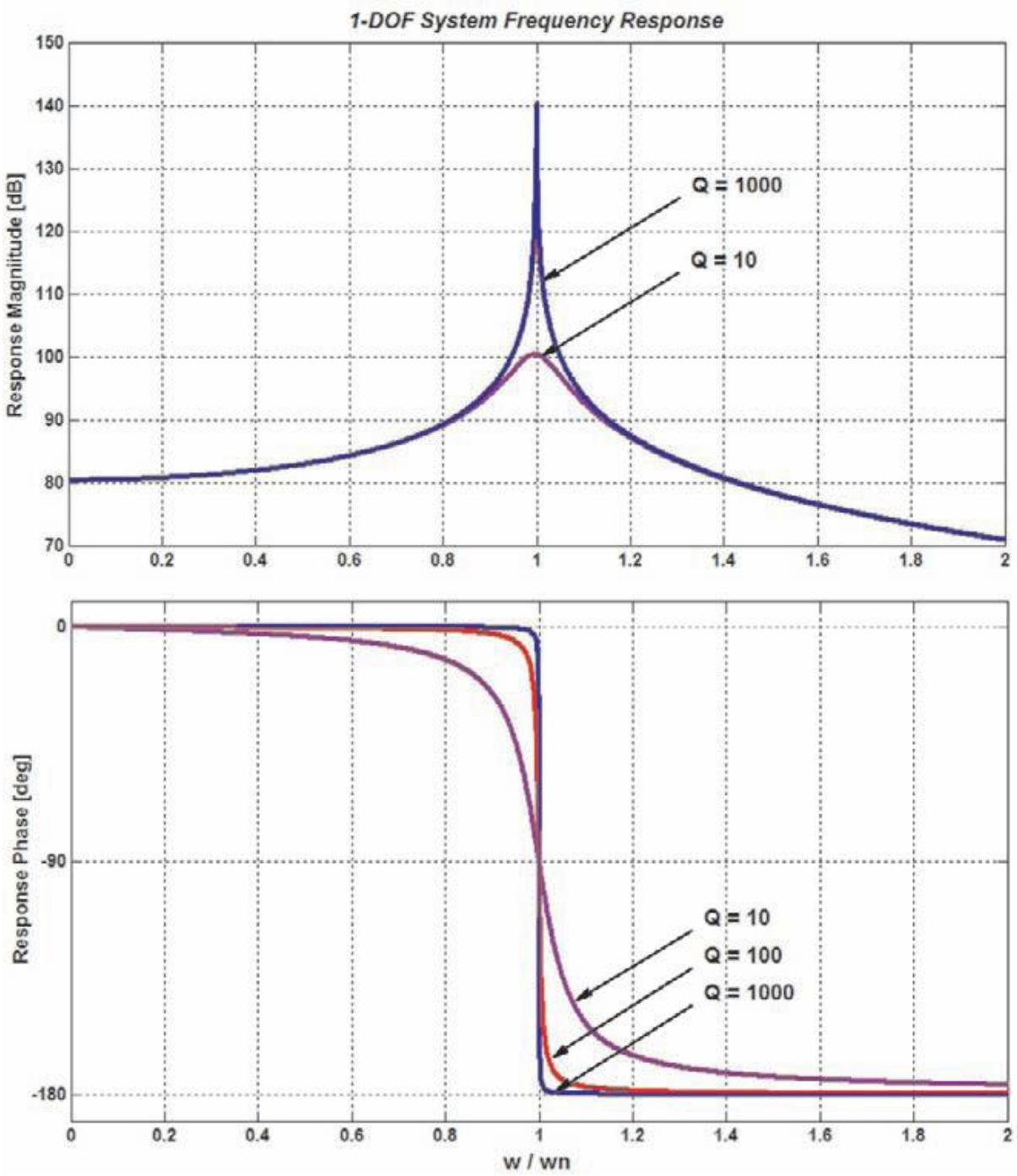

FIG-1.7 The Bode plot of a typical 1-DOF resonator

1.3 Drive-Mode Operation:

Since the Coriolis effect is based on conservation of momentum, every gyroscopic system requires a mechanical subsystem that generates momentum. In vibratory gyroscopes, the drive-mode oscillator, which is comprised of a proof-mass driven into a harmonic oscillation, is the source of momentum. The drive-mode oscillator is most commonly a 1 degree-of-freedom (1-DOF) resonator, which can be modeled as a mass-spring-damper system consisting of the drive proof-mass m_d, the drive mode suspension system providing the drive stiffness k_d, and the drive damping c_d consisting of viscous and thermo-elastic damping. With a sinusoidal drive-mode excitation force, the drive equation of motion along the x-axis becomes

$$m_d\ddot{x} + c_d\dot{x} + k_d x = F_d \sin \omega t \tag{1.26}$$

With the definition of the drive-mode resonant frequency w_d and the drive-mode Quality factor Q_d the amplitude and phase of the drive-mode steady-state response $x = x_0 \sin(\omega t + \phi_d)$ becomes:

$$x_0 = \frac{F_d}{k_d \sqrt{\left[1 - \left(\frac{\omega}{\omega_d}\right)^2\right]^2 + \left[\frac{1}{Q_d}\frac{\omega}{\omega_d}\right]^2}}$$

(1.27)

$$\phi_d = -\tan^{-1} \frac{\frac{1}{Q_d}\frac{\omega}{\omega_d}}{1 - \left(\frac{\omega}{\omega_d}\right)^2}$$

(1.28)

Where

$$\omega_d = \sqrt{\frac{k_d}{m_d}} \tag{1.29}$$

$$Q_d = \frac{m_d \omega_d}{c_d} \tag{1.30}$$

The scale factor of the gyroscope is directly proportional to the drive-mode oscillation amplitude. The phase and the frequency of the drive oscillation directly determines the phase and the frequency of the Coriolis force, and subsequently the sense-mode response. Thus, it is extremely critical to maintain a drive-mode oscillation with stable amplitude, phase and frequency.

1.4 The Coriolis Response:

The Coriolis response in the sense direction is best understood starting with the assumption that the drive-mode is operated at drive resonant frequency wd, and the drive motion is amplitude regulated to be of the form $x = x_0 \sin(\omega_d t + \phi_d)$ with a constant amplitude x0. The Coriolis force that excites the sense-mode oscillator is

$$F_C = -2m_C\Omega_z\dot{x} = -2m_C\Omega_z x_0 \omega_d \cos(\omega_d t + \phi_d)$$

(1.31)

Where m_C is the portion of the driven proof mass that contributes to the Coriolis force. In a simple single-mass design, m_C is usually equal to m_d. Here it should be emphasized again that the Coriolis force amplitude, which sets the scale factor of the gyroscope, is directly proportional to the drive-mode oscillation amplitude. Thus, the drive amplitude has to be well regulated to achieve a stable scale factor.

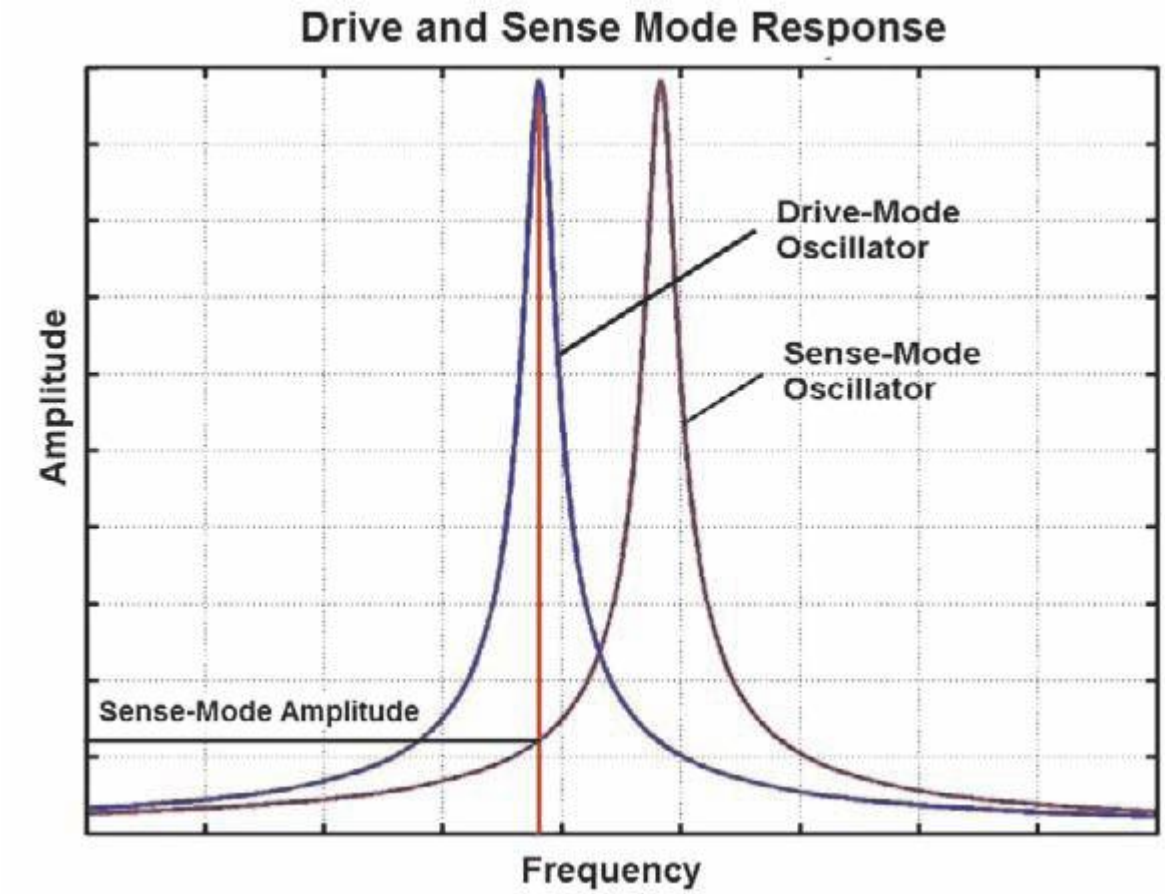

Fig. 1.8 The complete gyroscope system can be viewed as a combination of a 1-DOF drive-mode oscillator and a 1-DOF sense-mode oscillator.

Similar to the drive-mode oscillator, the sense-mode oscillator is also often a 1-DOF resonator. The primary reason for utilizing a 1-DOF resonator as the sensemode Coriolis accelerometer is to take advantage of resonance to amplify the mechanical response to the Coriolis force. The equation of motion of the 1-DOF sense mode oscillator is

$$m_s\ddot{y} + c_s\dot{y} + k_s y = -2m_C x_0 \omega_d \Omega_z \cos(\omega_d t + \phi_d) \tag{1.32}$$

where ms is the portion of the proof-mass that responds to the Coriolis force. Again, in a simple single-mass design, m_c ,m_d *and* m_s are equal. The amplitude and phase of the steady-state sense-mode Coriolis response in a linear system, defining the sense-mode resonant frequency w_s and the sense-mode Quality factor Q_s. Investigating the resonant

amplitude of the sense-mode Coriolis response, the sensitivity of the gyroscope to the angular rate input Wz can be improved by

- Increasing the drive-mode oscillation amplitude X_0
- Increasing Qs by decreasing damping, usually by vacuum packaging
- Maximizing the mass m_c that generates the Coriolis force, while minimizing the total mass ms excited by the Coriolis force.

In torsional systems, the fundamental resonant operation principle is the same as linear systems. Similarly, if we assume an amplitude regulated torsional drive motion of the form

$$\theta_d = \theta_d^{\circ} \sin(\omega_d t + \angle\theta_d) \tag{1.33}$$

the steady-state sense-mode Coriolis response, with f being the detected deflection angle about the sense axis for angular rate measurement, can be expressed as

$$\phi = \phi^{\circ} \sin(\omega_d t + \angle\phi) \tag{1.34}$$

1.4.1 Mode-Matching and Δf:

Even though matching the drive and sense-mode resonant frequencies greatly enhances the sense-mode mechanical response to angular rate input, it comes with many disadvantages. Operating close to the sense resonant peak also makes the system very sensitive to variations in system parameters that cause a shift in the resonant frequencies or damping. To illustrate this effect, let us consider a sense-mode system with a resonant frequency of w_s = 10kHz and a Q factor of Qs = 1000 (Figure 1.9). When the operating frequency matches the sense-mode resonant frequency ws the amplification factor is 1000, equal to the Q factor. If there is only 5Hz relative shift between the operating frequency and the sense-mode resonant frequency, the gain drops by 29.3%. For a 10Hz relative shift, the gain drop is 55%. Under higher quality factor conditions the gain is higher, however, the bandwidth becomes even narrower. For example, let us take the same sense-mode system with a resonant frequency of Ws = 10kHz, and increase the Q

factor to Qs = 10;000 (Figure 2.11). The amplification factor at resonance directly increases to 10,000. However, the half-power bandwidth becomes:

$$BW = \frac{\omega_s}{Q_s} = \frac{10,000\text{Hz}}{10,000} = 1\text{Hz}$$

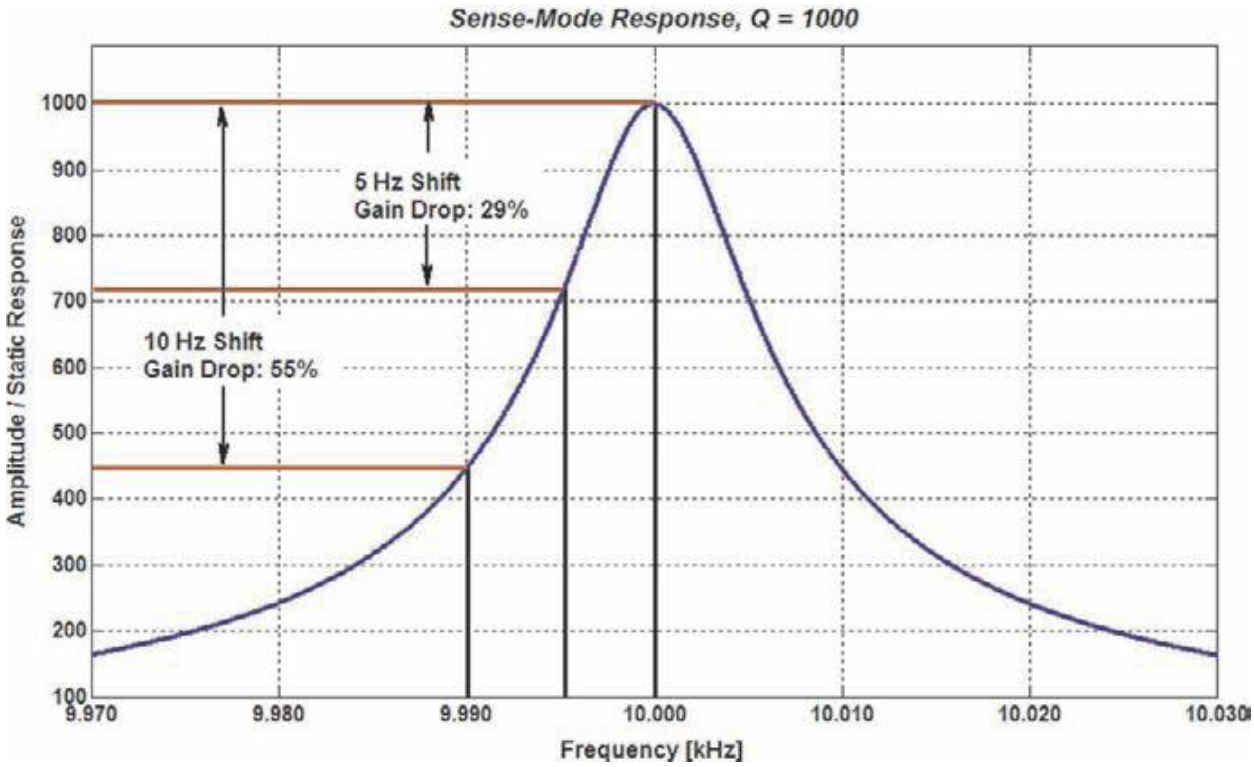

Fig. 1.9 The sense-mode amplification of a sense-mode system with a resonant frequency of w_s = 10kHz and a Q factor of Qs = 1000. For a 5Hz relative shift between the operating frequency and the sense-mode resonant frequency, the gain drop is 29%.

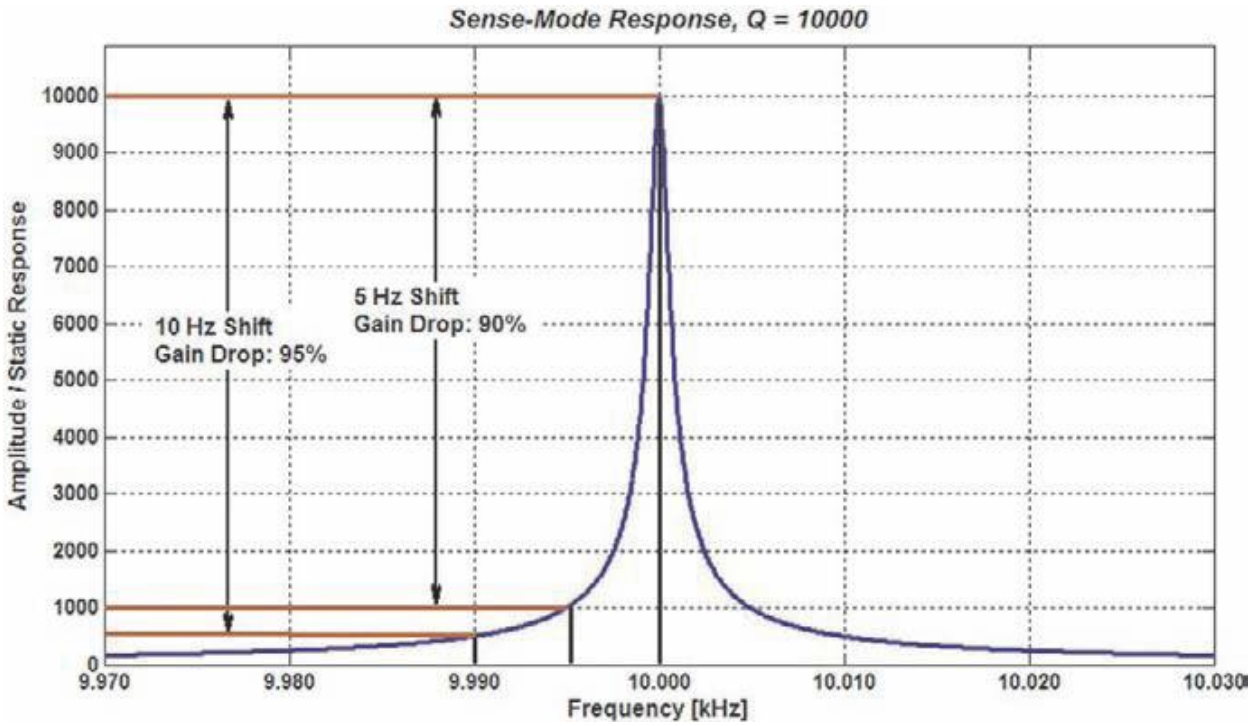

Fig. 1.10 High quality factor devices provide higher gains, but become more sensitive to frequency variations.

The sense-mode amplification of a system with Ws = 10kHz and Qs = 10;000 drops by over 90% for a 5Hz relative shift between the operating frequency and the sense-mode resonant frequency. This means that for only 0.5Hz mismatch, the gain drops by $1/\sqrt{2}$ i.e. 29.3%. If the mismatch is 5Hz, which is only 0.05% of the 10kHz resonant frequency, the gain drops by 90%.

1.4.2 Phase Relations and Proof-Mass Trajectory:

As explained in previous sections, the drive-mode oscillator is usually operated at resonance, and the drive-mode position phase is -90º relative to the drive AC signal. However, the sense-mode position phase depends heavily on the drive and sense frequency separation Δf , and damping. In the steady state, the drive-mode position is of the form.

$$x(t) = x_0 \sin(\omega_d t + \phi_d) \tag{1.35}$$

The drive-mode velocity can also be expressed as a sine signal, by taking the time derivative of the position and inverting the sign of cosine, resulting in a 90 º phase shift from the drive position

$$\dot{x}(t) = x_0 \omega_d \cos(\omega_d t + \phi_d) = x_0 \omega_d \sin(\omega_d t + \phi_d + 90^\circ) \quad (1.36)$$

The Coriolis force generated by the drive-mode oscillator will also be a sine signal at the same frequency and phase. The Coriolis force in the positive direction can be obtained by adding a -180 º phase shift.

1.5 Gyroscope Bias Stability (In-run Bias)

Definition:

Gyroscope Bias Stability (In-run Bias) is defined as the variation with time, of the residual bias error after compensation for a continuously powered IMU operating under stable conditions.

Measurement method:

Bias stability is the Standard Deviation of at least 60 consecutive *Bias Error* measurements taken from an IMU at stable conditions (after warm up). Each $Bias_{stability}$ measurement shall be taken as the 4-second average bias measured from 1 hour after IMU power up. The time allowed for warm up should be sufficiently long to ensure that there is no contribution due to start up (warm up) effects. These measurements will be made with the IMU at ambient temperature.

1.6 Gyroscope Bias Instability and Noise Floor:

Definition:

Gyroscope Bias Instability is a measure of the random variation of bias, characterised with a particular Correlation Time, CT. The noise is generally characterised by a 1/f power spectral density. This error is expressed as a Standard Deviation in units of °/s or °/h.

Measurement method:

Bias Instability for each axis, is measured using the Allan Variance method with the IMU in a static condition, after an appropriate warm up period (to achieve stable operation). The Allan Variance method is a time domain analysis technique used to determine the character of the random processes which give rise to the data noise. The process is described in more detail later in this Document.

Data is collected from the IMU over a period of at least 10 minutes. To reduce the amount of data collected, the IMU data for each channel may be averaged over a number samples but the averaging period should not be longer than 1 second.

The Allan Variance Chart is generated from the data, plotting the Standard Deviation of the *Bias Error* (1 sigma) versus Correlation Time, CT. The *Bias Instability* is obtained from flat part of the Allan Variance Chart where the plot provides the lowest bias, divided by 0.664.

Note that under some circumstances, the lowest point may not be flat and may be dominated by the intersection of the –0.5 and +0.5 gradients for the Angle Random Walk and the Rate Random Walk noise characteristics. Under such circumstances, the above method is a measure of the noise floor of the gyroscope rather than *Bias Instability.*

1.7 Allan Variance Definitions and Measurement Methods:

Allan Variance method

The Allan Variance Method is a time domain analysis technique used to determine the character of the random processes, which gives rise to data noise. Potentially, the technique can be applied to any instrument. When used to assess Gyroscopes, the technique can be used to determine Angle Random Walk and Bias Stability. When used to assess Accelerometers, the technique can be used to determine Velocity Random Walk and Bias Stability. The Allan Variance Method consists of a number of stages:

Stage 1: Data Collection

N samples of data, ω is collected from the instrument over a period of time, with a sampling frequency of f_0. To reduce the amount of data collected, the IMU data may be averaged over a number samples (during collection) but the averaging period should not be longer than 1 second (ie. at less than 1Hz).

Stage 2: Averaging Data

From the collection of *N* data points, a total of *K* (=*N*/*M*) data clusters are formed, where *M* is the number of consecutive samples in each cluster. The average for each cluster is then computed:

$$\varpi_k(M) = \frac{1}{M}\sum_{l=1}^{M}\omega_{(k-1)M+l} \qquad k=1,2.....\ K \qquad (1.37)$$

Stage 3: Compute Allan Variance

The Allan variance is calculated from the cluster averages:

$$\sigma_A^2(\tau_M) = \frac{1}{2}\left\langle\left[\varpi_{k+1}(M)-\varpi_k(M)\right]^2\right\rangle \quad \text{or}$$

$$\sigma_A^2(\tau_M) \cong \frac{1}{2(K-1)}\sum_{k=1}^{K-1}\left[\varpi_{k+1}(M)-\varpi_k(M)\right]^2 \qquad (1.38)$$

The $\langle\ \rangle$ symbols denote the average for each ensemble and τ_M ($=M/f_n$) is known as the Correlation Time.

Stage 4: Plot Allan Variance Chart

The Allan Variance Chart is then produced by plotting the Standard Deviation, σ against the Correlation Time, τ_M ,on a log-log scale.

1.8 Atlantic Inertial Systems:

The purpose of this document is to aid the user to install and operate the SiRRS01® single axis rate sensor. The Product Specification RRS01-00-0100PS defines the performance and operational environment parameters for the SiRRS01®, and is subject to revision.

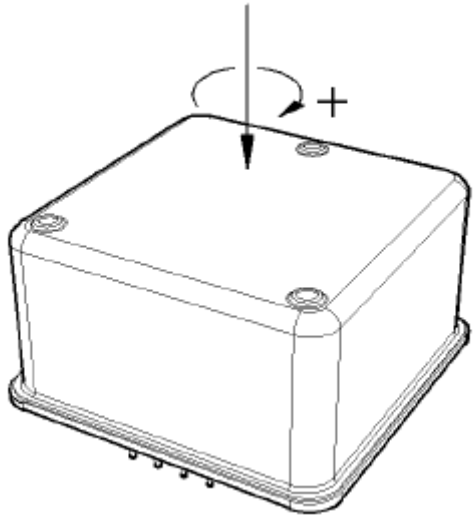

FIG- 1.11 SiRRS01®

Technical Specification Compliance features:

Key features of the SiRRS01® include:

• Wide measurement ranges

• Simple to use

• DC Input/DC Output

• Rapid start up (<300ms)

• High shock survival

• Low power

• Long life and maintenance free

1.8.1 Description:

The SiRRS01® is a solid state, single axis, angular rate sensor. It provides an analogue DC voltage output proportional to the rate of turn about its sensitive axis, and requires only a bipolar DC power supply for operation.

The sensitive axis is perpendicular to the base of the sensor, see Figure 1.11. The SiRRS01® is designed to be mounted using either adhesive (for long term installation) or clamps (short term). The SiRRS01® rate sensor is a hermetically sealed unit. The sensor housing is made from an all Kovar® metal construction, which is evacuated and dry-filled with nitrogen.

External connections are via nine pins on one face. Each sensor is digitally programmed for scale factor and bias, and is functionally tested over the full operating temperature range.

1.8.2 The SiRRS01® Rate output:

The SiRRS01® Rate output is measured with respect to the Rate Reference pin. It is recommended that a Differential Input Amplifier is used as a receiver device. The output saturates at approximately 2.2 V DC, but the performance is not specified above 2.0 V DC. The SiRRS01® Rate output impedance, load resistance and load capacitance are defined in Table 1, Table 2 and Table 3 External Load Resistance respectively.

Table: 1 **Rate Output Impedance**

Minimum	Typical	Maximum
0Ω	5 Ω	15 Ω

Table: 2 **External Load Resistance**

Minimum	Maximum
10K Ω	∞ Ω

Table: 3 External Load Capacitance

Minimum	Maximum
0	10 nF

Table: 4

The specifications of the Rate Sensor Gyro – RRS01-03-0100 are given in the following Table:4

S. NO	**Parameter**	**Specification given by RCI**	**Specification of Rate SensorGyro quoted by Akash Technologies (Manufacturer: Atlantic Inertial Systems, UK)**	**Compliance**
1	Range	+/- 300 °/s	+/- 300 °/Sec	Complied
2	Scale Factor Linearity	+/- 1% of FS	Less than or equal to +/- 1%	Complied
3	Scale Factor Repeatability	0.05% 1σ	0.05% 1σ	Complied
4	Bias Stability	3 °/hr 1σ	Bias instability typically less than 5.5 °/hr	
5	Bias Repeatability	0.030/s 1σ	0.030/s 1σ	Complied
6	Band Width	> 50 Hz	> 50 Hz	Complied

7	Random Walk	0.20 °/√hr	Typically less than 0.26 °/√hr	
8	Operating Temperature	-40 °C To +75 °C	-40 °C To +75 °C	Complied
9	Vibration	10 grms, 20-2000 Hz	10 grms, 20-2000 Hz	Complied
10	Shock	100 g 11 msec	1000 g 1ms, 60g 30 msec	
11	Humidity	100% RH	95% RH	
12	Weight	< 50 grams	< 35 grams	Complied
13	Power	< 5 VA	< 0.5 VA	Complied

Table : 5

The specifications of the Rate Sensor Gyro – RRS01-01-0100 are given in the following

S. No.	**Parameter**	**Specification given by RCI**	**Specification of Rate Sensor Gyro quoted by Akash Technologies (Manufacturer: Atlantic Inertial Systems, UK)**	**Compliance**
1	Range	+/- 110 °/s	+/- 110 °/s	Complied
2	Scale Factor Linearity	+/- 1% of FS	Less than or equal to +/- 1%	Complied
3	Scale Factor Repeatability	0.05% (1)	0.05% (1)	
4	Bias Stability	3 °/hr (1)	Bias instability typically less than 5.5 °/hr	Complied

5	Bias Repeatability	0.030/s (1)	0.030/s (1)	
6	Band Width	> 50 Hz	> 50 Hz	Complied
7	Random Walk	0.20 °/√hr	Typically less than 0.26 °/√hr	
8	Operating Temperature	-40 °C To +75 °C	-40 °C To +75 °C	Complied
9	Vibration	10 grms, 20-2000 Hz	10 grms, 20-2000 Hz	Complied
10	Shock	100 g 11 msec	1000 g 1ms, 60g 30 msec	Complied
11	Humidity	100% RH	95% RH	
12	Weight	< 50 grams	< 35 grams	Complied
13	Power	< 5 VA	< 0.5 VA	Complied

1.9 Summary:

Explaining the basics of the drive and sense-mode oscillators, it was illustrated that the performance of the gyroscope is very sensitive to variations in system parameters that shift the drive or sense resonant frequencies. Under high quality factor conditions the gain is high, however, the bandwidth is extremely narrow, which also results in abrupt phase changes. The Product Specification RRS01-00-0100PS defines the performance and operational environment parameters for the SiRRS01.

CHAPTER 2

Fundamentals of Wavelet Transform

2.1 Introduction to wavelet

The a-periodic, noisy, transient signals are the type of signals for which wavelet transforms are particularly useful. Wavelets have the ability to examine signals simultaneously in both time and frequency domain. Current applications of wavelet include climate analysis, heart monitoring, condition monitoring of rotating machinery, seismic de-noising, de-noising of astronomical images, and characterization of turbulent intermittency, and so on.

Wavelet means 'small wave'. So, wavelet analysis is about analyzing signal with short duration finite energy functions. They transform the signal under investigation into another representation which presents the signal in more useful form. This transformation of the signal is called wavelet transform. There are a variety of wavelets that are used for signal analysis.

Choice of a particular wavelet depends on the type of application. Wavelets can be manipulated in two ways. The first one is translation. We change the central position of the wavelet along the time axis. The second one is scaling. Figures given below, show translated and scaled versions of wavelets.

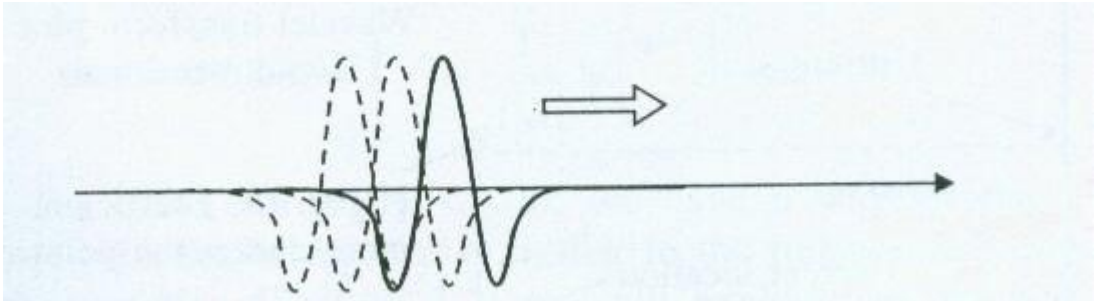

Figure 2.1 Translation of wavelets.

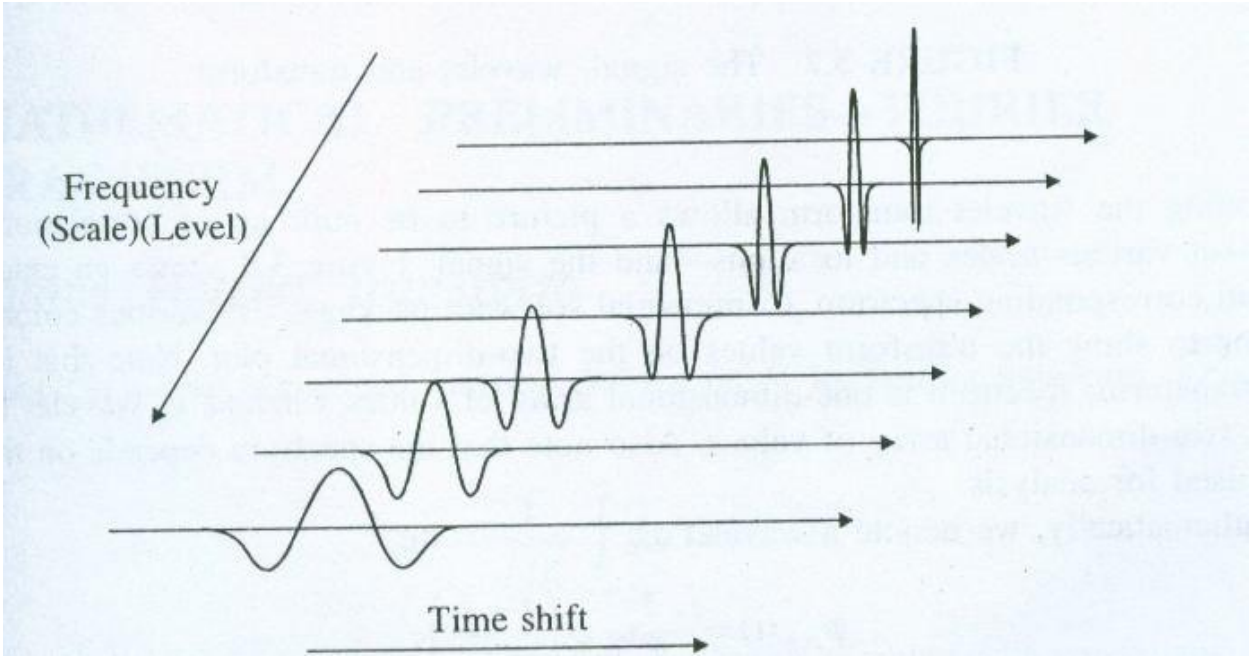

Figure 2.2 Change in scale of wavelet.

Figure 2.3 shows a schematic of the wavelet transform which basically quantifies the local matching of the wavelet with the signal. If the wavelet matches the shape of the signal well at a specific scale and location, as it happens to do in top plot of the figure (2.3), then a large transform value is obtained. The transform value is then plotted in the two –dimensional transform plane shown at the bottom of the figure (2.3). The transform is computed at various locations of the signal and for various scales of the wavelet. If the process is done in a smooth and continuous fashion then the transform is called continuous wavelet transform. If the scale and position are changed in discrete steps, the transform is called discrete wavelet transform.

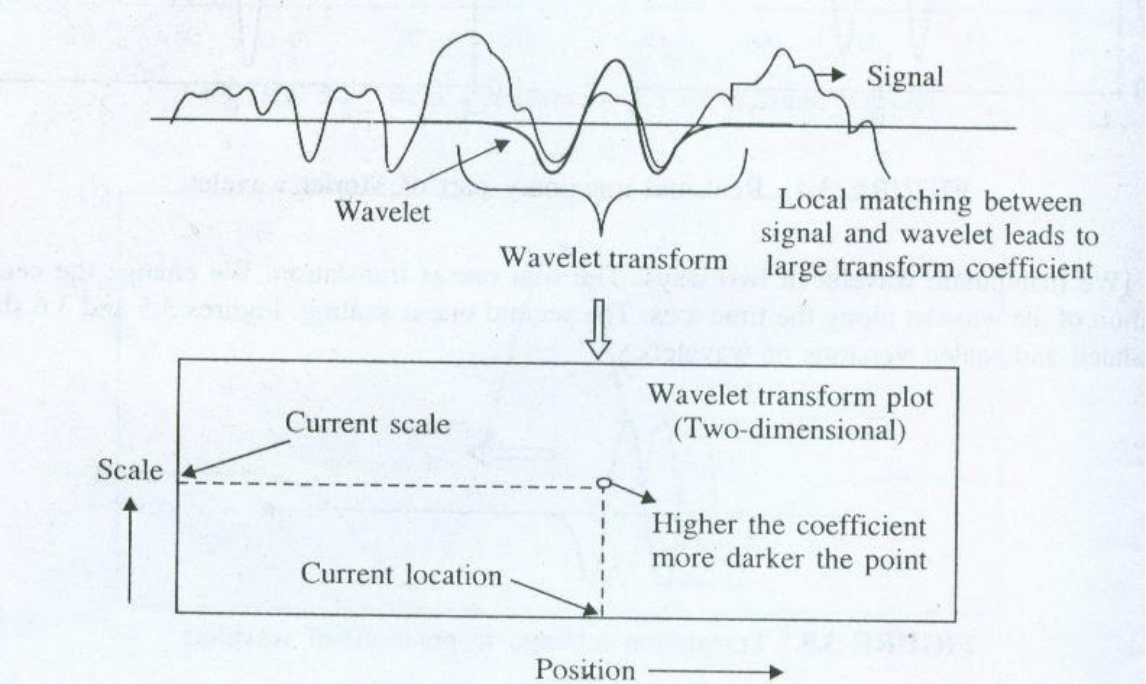

Figure 2.3 The signal, wavelet and transform

Mathematically, wavelet is denoted as:

$$\Psi_{a,b}(t) = 1/\sqrt{|a|} * \psi(t-b)/a$$

Where b is location parameter and a is scaling parameter. For the function to be a wavelet, it should be time limited. For a given scaling parameter a, we translate the wavelet by varying the parameter b.

The wavelet transform can be defined as:

$$W(a, b) = \int f(t) * 1/\sqrt{|a|} * \psi(t-b)/a \, dt$$

According to Equation 2.2, for every (a, b), we have a wavelet transform coefficient, representing how much the scaled wavelet is similar to the function f (t) at location t = b/a. Our goal is to generate a set of expansion functions such that any signal can be represented by the Series

$$f(t) = \sum_{a,\,b} \Phi_{a,b}\, 2a^{/2}\ \psi(2^{a/2} - b)$$

Where the two dimensional set of coefficients Φa, b is called discrete wavelet transform (DWT) of f(t).

A wavelet is a waveform of effectively limited duration that has an average value of zero. Compare wavelets with sine waves, which are the basis of Fourier analysis. Sinusoids do not have limited duration , they extend from minus to plus infinity. And where sinusoids are smooth and predictable, wavelets tend to be irregular and asymmetric. Fourier analysis consists of breaking up a signal into sine waves of various frequencies. Similarly, wavelet analysis is the breaking up of a signal into shifted and scaled versions of the original (or mother) wavelet.

It also makes sense that local features can be described better with wavelets that have local extent. Wavelets have scale aspects and time aspects, consequently every application has scale and time aspects. To clarify them we try to untangle the aspects somewhat arbitrarily.

For scale aspects, we present one idea around the notion of local regularity. For time aspects, we present a list of domains. When the decomposition is taken as a whole, the de-noising and compression processes are center points.

2.1.1. Scale Aspects:

As a complement to the spectral signal analysis, new signal forms appear. They are less regular signals than the usual ones. The cusp signal presents a very quick local variation. Its equation is with t close to 0 and $0 < r < 1$. The lower r the sharper the signal. To illustrate this notion physically, imagine you take a piece of aluminum foil; The surface is very smooth, very regular. You first crush it into a ball, and then you spread it out so that it looks like a surface. The asperities are clearly visible. Each one represents a two-dimension cusp and analog of the one dimensional cusp. If you crush again the foil, more tightly, in a more compact ball, when you spread it out, the roughness increases and the regularity decreases.

Several domains use the wavelet techniques of regularity study:

- Biology for cell membrane recognition, to distinguish the normal from the pathological membranes
- Metallurgy for the characterization of rough surfaces
- Finance (which is more surprising), for detecting the properties of quick variation of values
- In Internet traffic description, for designing the services size

2.1.2 Time Aspects:

Let's switch to time aspects. The main goals are

- Rupture and edges detection
- Study of short-time phenomena as transient processes

As domain applications, we get

- Industrial supervision of gear-wheel Checking undue noises in craned or dented wheels, and more generally in nondestructive control quality processes.
- Detection of short pathological events as epileptic crises or normal ones as evoked potentials in EEG (medicine)
- SAR imagery
- Automatic target recognition
- Intermittence in physics

2.2 Wavelets and filters

The method of averaging and differencing explained above can also be expressed as *filtering* the data. Averaging corresponds to a low pass filtering. It removes high frequencies of the data. Since details (sharp changes in the data) correspond to high frequencies, the averaging procedure tends to smooth the data. The low pass filter can be expressed as $1/\sqrt{2}$ (1,1) in the Haar case and when we average the data, we move this filter along our input data.

The differencing corresponds to high pass filtering. It removes low frequencies and responds to details of an image since details correspond to high frequencies. It also responds to noise in an image, since noise usually is located in the high frequencies. The high pass filter can be expressed as $1/\sqrt{2}$ (1,1) in the Haar case and when we difference the data, we simply move this filter along our input data. The low pass and high pass filters make up what in signal processing language is referred to as a *filter bank*. The method of averaging and differencing is referred to as analysis. The reverse procedure (going the opposite way in the example above) is called synthesis.

Hence, the wavelet transform separates low and high frequencies, just as the Fourier transform. Since different features of a signal (background, details, noise, edges, etc.) correspond to different frequencies, this is a key to use wavelets in signal processing. The nice thing is that wavelets are localized since they only live on part of the interval of the data, as opposed to the trigonometric functions used in Fourier analysis which live on the entire interval of the data.

2.2.1 Wavelet Decomposition as a Whole:

Many applications use the wavelet decomposition taken as a whole. The common goals concern the signal or image clearance and simplification, which are parts of de-noising or compression. We find many published papers in oceanography and earth studies. One of the most popular successes of the wavelets is the compression of fingerprints.

When trying to classify the applications by domain, it is almost impossible to sum up several thousand papers written within the last 15 years. Moreover, it is difficult to get information on real-world industrial applications from companies. They understandably protect their own information. Some domains are very productive. Medicine is one of them. We can find studies on micro-potential extraction in EKGs, on time localization of His bundle electrical heart activity, in ECG noise removal. In EEGs, a quick transitory signal is drowned in the usual one. The wavelets are able to determine if a quick signal exists, and if so, can localize it. There are attempts to enhance mammograms to discriminate tumors from calcifications.

2.3 Wavelet Analysis:

Wavelet analysis is becoming a common tool for analyzing localized variations of power within a time series. By decomposing a time series into time–frequency space, one is able to determine both the dominant modes of variability and how those modes vary in time.
Wavelet analysis represents the next logical step: a windowing technique with variable-sized regions. Wavelet analysis allows the use of long time intervals where we want more precise low-frequency information, and shorter regions where we want high-frequency information.

FIG- 2.4 time-based , frequency based and STFT signal

Here's what this looks like in contrast with the time-based, frequency-based, and STFT views of a signal:

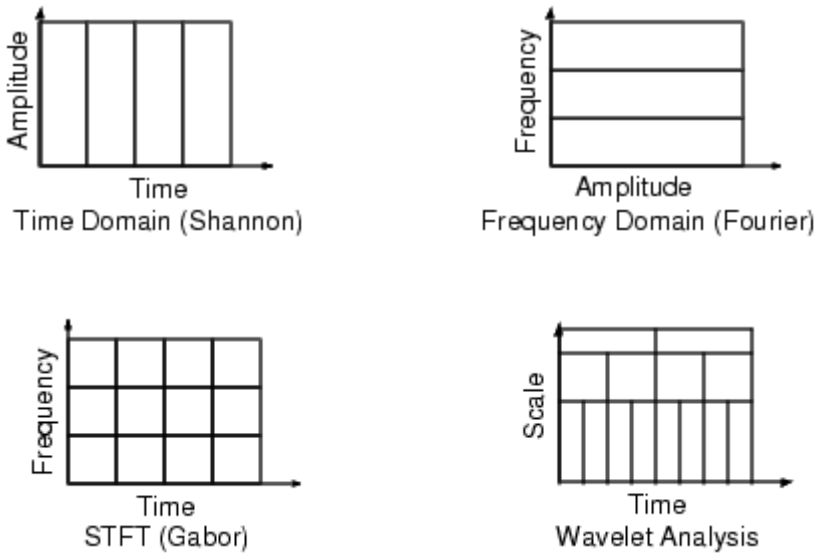

We may have noticed that wavelet analysis does not use a time-frequency region, but rather a time-scale region.

Wavelet analysis is capable of revealing aspects of data that other signal analysis techniques miss, aspects like trends, breakdown points, discontinuities in higher derivatives, and self-similarity. Furthermore, because it affords a different view of data than those presented by traditional techniques, wavelet analysis can often compress or de-noise a signal without appreciable degradation.

Indeed, in their brief history within the signal processing field, wavelets have already proven themselves to be an indispensable addition to the analyst's collection of tools and continue to enjoy a burgeoning popularity today.

2.4 The Discrete Wavelet Transform:

Calculating wavelet coefficients at every possible scale is a fair amount of work, and it generates an awful lot of data. What if we choose only a subset of scales and positions at which to make our calculations?

It turns out, rather remarkably, that if we choose scales and positions based on powers of two so called dyadic scales and positions, then our analysis will be much more efficient

and just as accurate. We obtain such an analysis from the discrete wavelet transform (DWT).

One-Stage Filtering: Approximations and Details

For many signals, the low-frequency content is the most important part. It is what gives the signal its identity. The high-frequency content, on the other hand, imparts flavor or nuance. Consider the human voice. If you remove the high-frequency components, the voice sounds different, but you can still tell what's being said. However, if you remove enough of the low-frequency components, you hear gibberish.

In wavelet analysis, we often speak of approximations and details. The approximations are the high-scale, low-frequency components of the signal. The details are the low-scale, high-frequency components.

The filtering process, at its most basic level, looks like this:

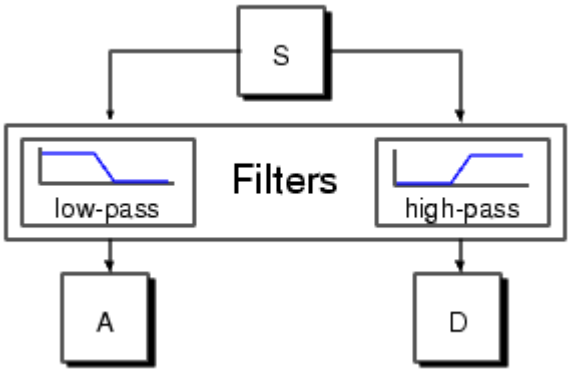

FIG_2.5 filtering process

The original signal, S, passes through two complementary filters and emerges as two signals.

Unfortunately, if we actually perform this operation on a real digital signal, we wind up with twice as much data as we started with. Suppose, for instance, that the original signal S consists of 1000 samples of data. Then the resulting signals will each have 1000 samples, for a total of 2000.

These signals A and D are interesting, but we get 2000 values instead of the 1000 we had. There exists a more subtle way to perform the decomposition using wavelets. By looking carefully at the computation, we may keep only one point out of two in each of the two 2000-length samples to get the complete information. This is the notion of downsampling. We produce two sequences called C_A and C_D.

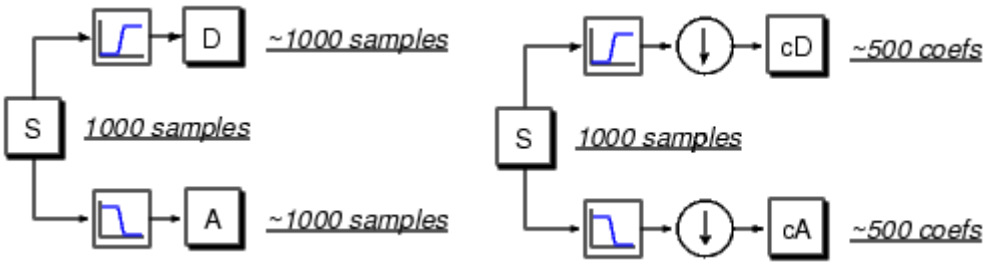

FIG-2.6 UP sampling and Down sampling DWT

The process on the right, which includes downsampling, produces DWT coefficients.To gain a better appreciation of this process, let's perform a one-stage discrete wavelet transform of a signal. Our signal will be a pure sinusoid with high-frequency noise added to it.

2.5 An Introduction to the Wavelet Families:

Several families of wavelets that have proven to be especially useful are included in this toolbox. What follows is an introduction to some wavelet families.

- Haar
- Daubechies
- Biorthogonal
- Coiflets
- Symlets
- Morlet
- Mexican Hat

- Other Real Wavelets
- Complex Wavelets

Here Haar and Daubechies are described because we are denoising the mems gyro data using these two wavelets.

2.5.1 Haar wavelets:

The Haar wavelet is the simplest wavelet.

$$w_H(x) = \begin{cases} 1 & 0 < x < 1/2 \\ -1 & 1/2 < x < 1 \\ 0 & \text{otherwise} \end{cases}$$

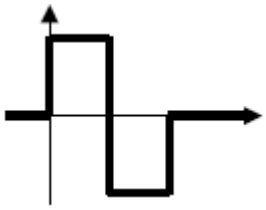

The mother wavelet obviously satisfies the two wavelet requirements, as it is both **local** and **oscillatory**. The picture below shows the shapes of Haar wavelets for various scales and translations.

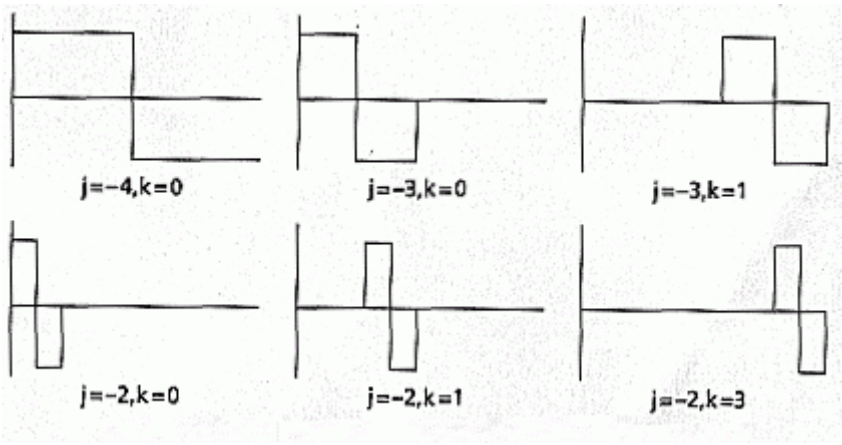

FIG_2.7 Haar wavelets for various scales and translations.

2.5.2 Daubechies wavelets

The **Daubechies wavelets** are a family of orthogonal wavelets defining a discrete wavelet transform and characterized by a maximal number of vanishing moments for some given support. With each wavelet type of this class, there is a scaling function (also called mother wavelet) which generates an orthogonal multi-resolution analysis.

The field of Discrete Wavelet Transform is a recent one. The complete theory and toolbox set has been developed in the 90's and nowadays is producing interesting results on signal compression systems. First of all a short introduction to the continuos wavelet transform (CWT) will be given: As well as the Fourier Transform uses a basis function , the CWT is based on other kind of basis functions which accomplish an interesting property: all of them are generated by dilation and shift of a single function j(t) (called a mother wavelet).

This kind of transform allows a non-uniform frequency resolution, just like the one obtained by the filter bank shown bellow

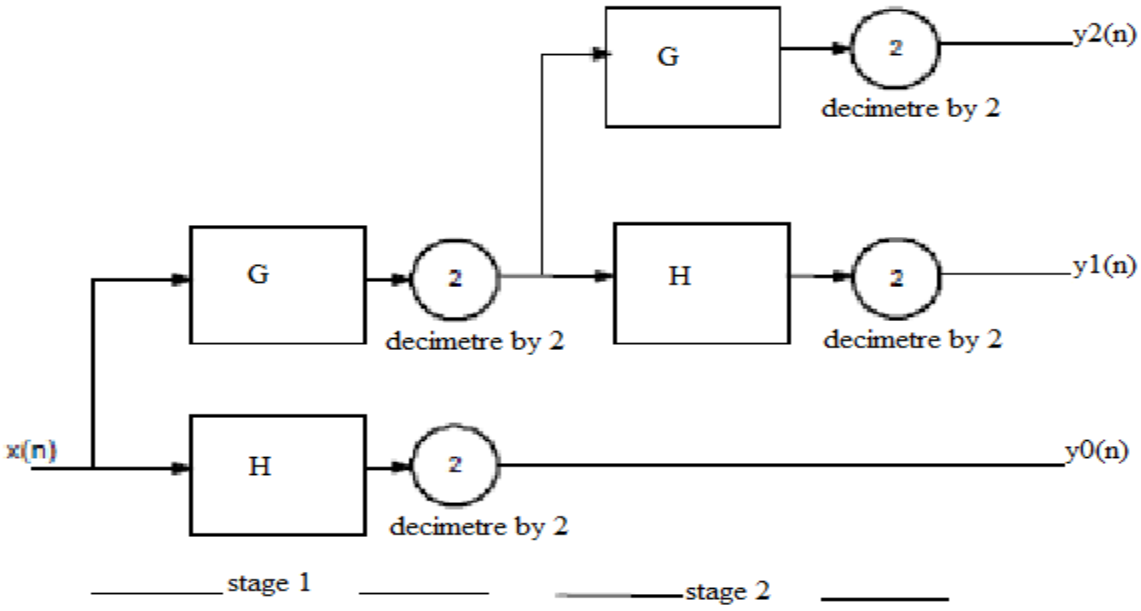

The second step is to discretize the expressions of CWT. which leads to a convolution like expression for both filters H (high pass) and G (low pass) and opens path to a digital implementation.

The last step was done by Daubechies in the 90's, who developed a systematic technique for generation of finite-length ortho-normal wavelet functions that has supposed a ultimate advance towards the building of wavelet transformers using finite impulse response (FIR) filters. The most important characteristic of the FIR filters obtained form Daubechies functions is that they are Power Symmetric, which allows us to implement those filters using a Lattice Structure. The Lattice Structure has many advantages, such as better coefficient quantization response as well as a reduction by a factor of two of the stages needed for a given filter order.

CHAPTER 3

PROPOSED METHOD

I have taken Haar wavelet transformation of the original signal at different levels and we got the wavelet coefficients of each level. Then the noise is estimated at each level. After estimation of noise, the threshold is calculated at each level and a shrinkage function is created. After applying the thresholding method we reconstruct the signal using inverse wavelet transform and get the de-noised signal. The flow chart is given below.

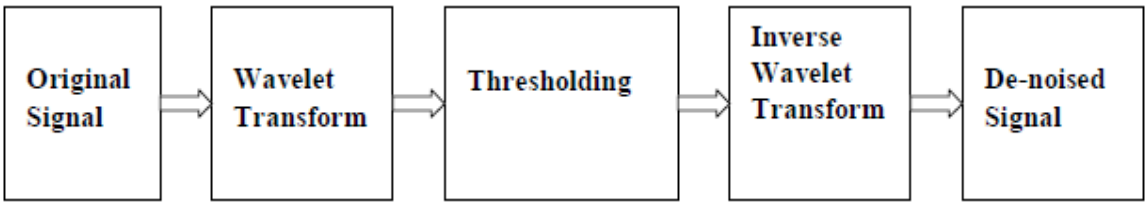

Figure 3.1 Flow Chart of De-Noising Method

3.1 Haar Wavelet Analysis:

The simplest possible orthogonal wavelet system is generated from the Haar scaling function and wavelet. Those are shown below.

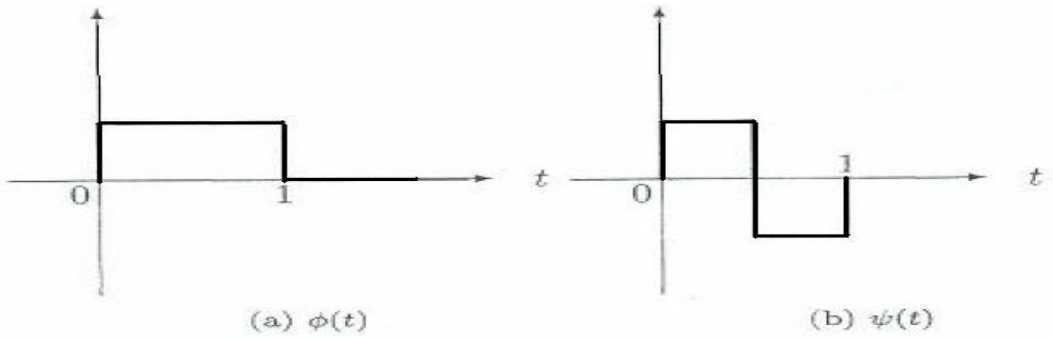

FIG 3.2 Haar scaling function and Wavelet

Haar scaling function Φ (t) is defined below. The domain of the function is [0, 1]. The function is time limited and has finite energy. That is, $\int |f(t)|^2$ exists and is finite.

$$\phi(t) = \begin{cases} 1 & \text{if } 0 < t < 1 \\ 0 & \text{otherwise} \end{cases}$$

(3.1)

The Haar wavelet function is defined as:

$$\psi(t) = \begin{cases} 1 & \text{if } 0<t<0.5 \\ -1 & \text{if } 0.5<t<1 \\ 0 & \text{Otherwise} \end{cases}$$

(3.2)

The combination of these scaling functions and wavelets allows a large class of signals to be represented by

$$\mathbf{f(t)} = \sum_{b} c_b \Phi (t - b) + \sum_{a,\,b} d_{a,\,b} \psi (2^{j/2} t - b)$$

(3.3)

3.2 **De-noising Using Wavelet Shrinkage Statistical Modeling and Estimation**

The smoothing removes high frequency components and retains low frequency components. Where as de-noising attempts to remove whatever noise is present and retains whatever signal is present regardless of the frequency content of the signal. The wavelet based de-noising process consists of three steps:

i) a linear forward wavelet transform

ii) a non-linear shrinkage de-noising

iii) a linear inverse wavelet transform

A noisy signal can be represented by

$$X_i(t) = S_i(t) + \sigma\varepsilon_i(t)$$

(3.4)

Where $X_i(t)$) is assumed to come from zero-mean normal distribution, $\varepsilon_i(t)$ is independent standard normal N(0,1) random variables and noise level σ is known or unknown. The goal is to recover the function S from the noisy data X. The three steps of de-noising using wavelet coefficient shrinkage technique are as follows:

Step – 1:

Calculate the wavelet coefficient matrix w by applying a wavelet transformation W to the data.

$$w = W(X) = W(S) + W(\sigma\varepsilon)$$

(3.5)

Step – 2:

Modify the wavelet coefficients of w to obtain the estimate w^ of the wavelet coefficients of S:

$$W \longrightarrow \overline{W}$$

(3.6)

Step – 3:

Inverse transform the modified wavelet coefficients to obtain the de-noised coefficients.

3.3 Noise Estimation:

Threshold methods can be classified into two categories: global threshold level dependent threshold. In global threshold method, we choose a single value for threshold λ to be applied globally to all wavelet coefficients while level dependent threshold means that a possibly different threshold value λj is chosen for each resolution level j. Donoho and Johnstone (1994) had suggested a robust estimation of σ in wavelet domain based only on the empirical wavelet coefficients at the finest resolution level. The reason for considering only finest level is that the corresponding empirical wavelet coefficients tend to consist mostly of noise. Since there is some signal present even at this level, Donoho

and Johnstone (1994) proposed a robust estimation of the noise level σ based on **Median Absolute Deviation (MAD)** given by

$$\overline{\sigma} = \frac{\text{Median}\{|w_k - \text{Median}(w_i)|: i, k = 1,2,3,\ldots\ldots,n/2\}}{0.6745} \qquad (3.7)$$

Where Wk, Wi are wavelet coefficient at the finest level. If we have started with n sampled data, after first level of filtering, we will have n/2 detail coefficients. Let w denotes a signal wavelet coefficient and w^ denotes its shrink version. Let λ be the threshold and Dλ(.) denotes the shrinkage function which determines how the threshold is applied to the data. Then

$$\overline{w} = \overline{\sigma} \, . \, D\lambda \, (w / \overline{\sigma}) \qquad (3.8)$$

Dividing w by σ^ we standardize the w coefficients to get w and to this standardized ws, we apply the threshold operator. After threshold, the resultant coefficients are multiplied with σ^ to obtain w^.

3.4 Median Absolute Deviation (MAD):

The median absolute deviation is one measure of statistical dispersion. It is a more robust and more general estimator of scale than the sample variance or standard deviation. In order to use the MAD as a consistent estimator for the estimation of the standard deviation σ, one takes

$$\hat{\sigma} = K \cdot \text{MAD} \qquad (3.9)$$

Where, *K* is a constant scale factor, which depends on the distribution. For normally distributed data *K* is taken to be

$$1 / \Phi^{(-3/4)} \approx 1/0.6745$$

Where, Φ is the **cumulative distribution function** for the standard normal distribution.

So, $\bar{\sigma} = MAD / 0.6745$ (3.10)

3.5 Threshold Selection:

The universal rule was proposed by Donoho and Johnstone as a global rule for onedimensional signals. For a signal of size n, the threshold is $\lambda = \sqrt{(2 \log n)}$

If data is not normalized with respect to noise-standard deviation, we estimate σ^ and use $\lambda = \bar{\sigma} \cdot \sqrt{(2 \log n)}$

3.6 Shrinkage Function:

The shrinkage function determines how the threshold is applied to the data. There are two types of shrinkage function and are given below.

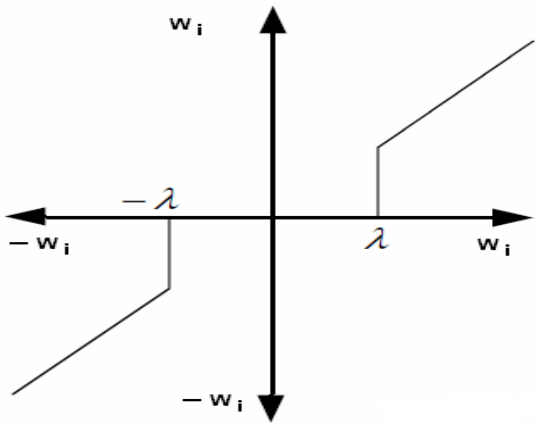

Figure 3.2a Hard Thresholding

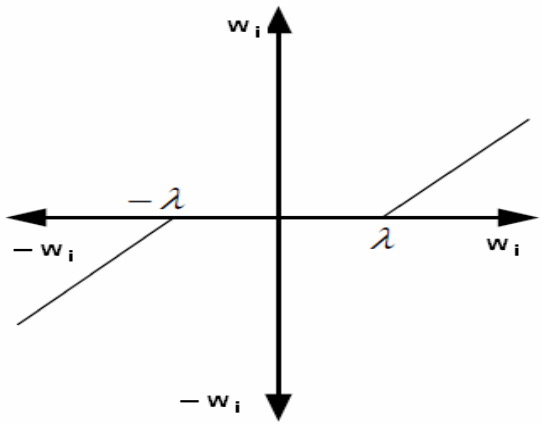

Figure 3.2b Soft Thresholding

a) Shrinkage function for hard threshold:

$$D^{\lambda}(w) = \begin{cases} w & \text{for all } |w| > \lambda \\ 0 & \text{Otherwise} \end{cases}$$

b) Shrinkage function for soft threshold:

$$D^{\lambda}(w) = \begin{cases} w - \lambda & \text{for all } w > \lambda \\ w + \lambda & \text{for all } w < -\lambda \\ 0 & \text{Otherwise} \end{cases}$$

CHAPTER 4

4.1 RESULTS

The chose of wavelet function and shrinkage function are important to the de-noising result. We have used Haar wavelet function and shrinkage function for soft threshold to de-noise the out put signal of gyro. The experiments were carried on data supplied by RCI, Hyderabad at different time and the experimental results are given below.

```
%  Wavelet program using soft thresholding for denoising
%Level 5 wavelet decomposition
% Developed by S K Das
% Version: 1  date : 19/04/2010

clear all;
close all;
load 'r3d_rat_run2.txt';
s=r3d_rat_run2;
l_s=length(s);

[cA1,cD1] = dwt(s,'haar');   % conduct descrete wavelet

A1 = upcoef('a',cA1,'haar',1,l_s);   % constuct approximation
D1 = upcoef('d',cD1,'haar',1,l_s);   % construct detailes output

subplot(1,2,1); plot(A1); title('Approximation A1');
subplot(1,2,2); plot(D1); title('ADetail A1');

A0 = idwt(cA1, cD1, 'haar', l_s);     % conduct inverse wavelet to regenerate the signal;
```

```
err = max(abs(s-A0));

% Perform multilevel wavelet decomposition

[C,L]  = wavedec(s,3,'haar');     % level 3 decomposition, vector L gives length s of each component


CA3=appcoef(C,L, 'haar', 3);     %  Extract approximation and detail coefficients

A3 = wrcoef('a', C, L, 'haar', 3);   %reconstruct level 3 approximation
D1= wrcoef('d', C, L, 'haar', 1);  % level 1 detail
D2= wrcoef('d', C, L, 'haar', 2);   % level 2 detail
D3= wrcoef('a', C, L, 'haar', 3);  % level 3 detail

% Display decompositions
figure;
subplot(2,2,1); plot(A3); title('Approximation A3');
subplot(2,2,2); plot(D1); title ('Detail D1');
subplot(2,2,3); plot(D2); title ('Detail D2');
subplot(2,2,4); plot(D3); title ('Detail D3');

A0 = waverec( C, L, 'haar');   % reconstruct original signal
% Compare original signal and reconstructed signal
figure;
subplot(2,1,1); plot(s); title('Original'); axis off
subplot(2,1,2); plot(A3); title('Level 3 appoximation'); axis off;

% DENOISING PROCESS

[thr,sorh,keepapp] = ddencmp ('den', 'wv', s);
```

```
clean = wdencmp('gbl', C, L, 'haar', 3, thr, sorh, keepapp);

figure;
subplot(2,1,1); plot(s(1:100)), title('Original');
subplot(2,1,2); plot(clean(1:100)), title('De-noised');

%plot(s), hold on, plot(clean, 'r-');
xd = wden(s, 'heursure', 's', 'mln', 5, 'haar');

figure;
plot(s), hold on, plot(xd,'r-')
std(s)
std(xd)
```

We got the result by de-noising of data of 3 degree moving vehicle as follows

ans = 19.1128

ans = 3.8315

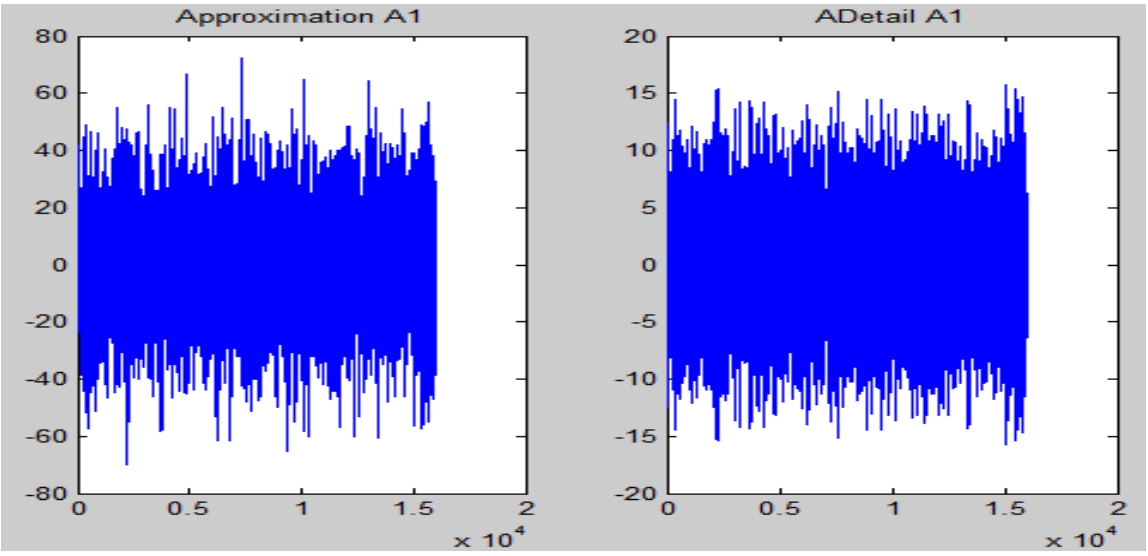

FIG_4.1(A) Approximation Haar de-noising

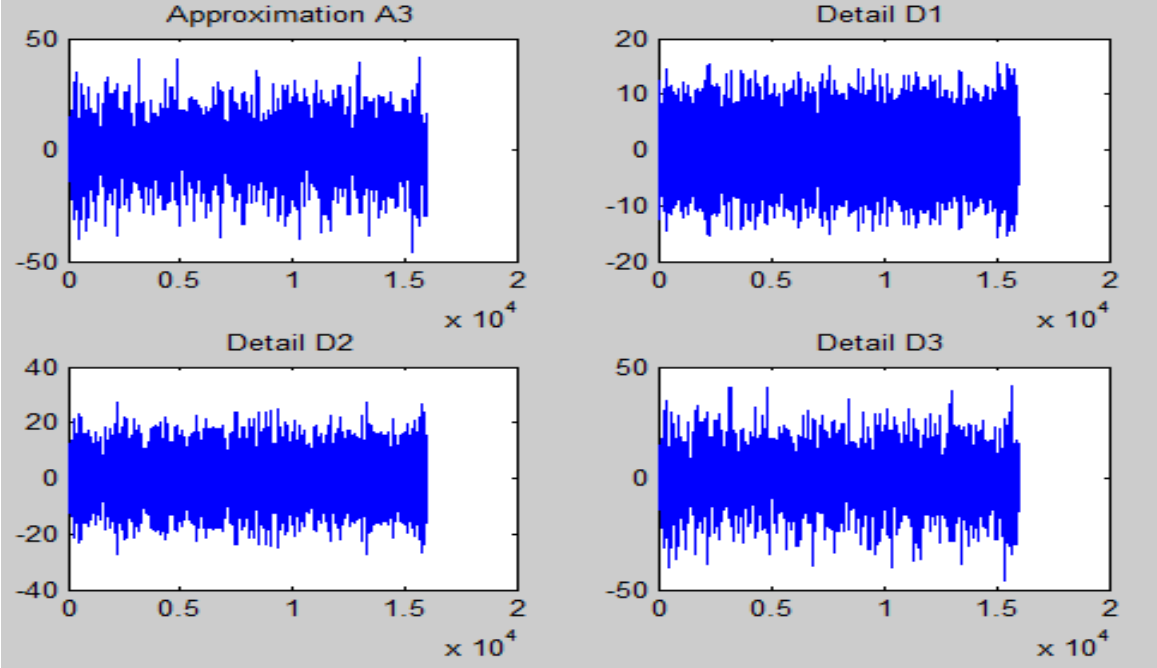

FIG_4.1(B) decompose Approximation level 3 of Haar de-noising

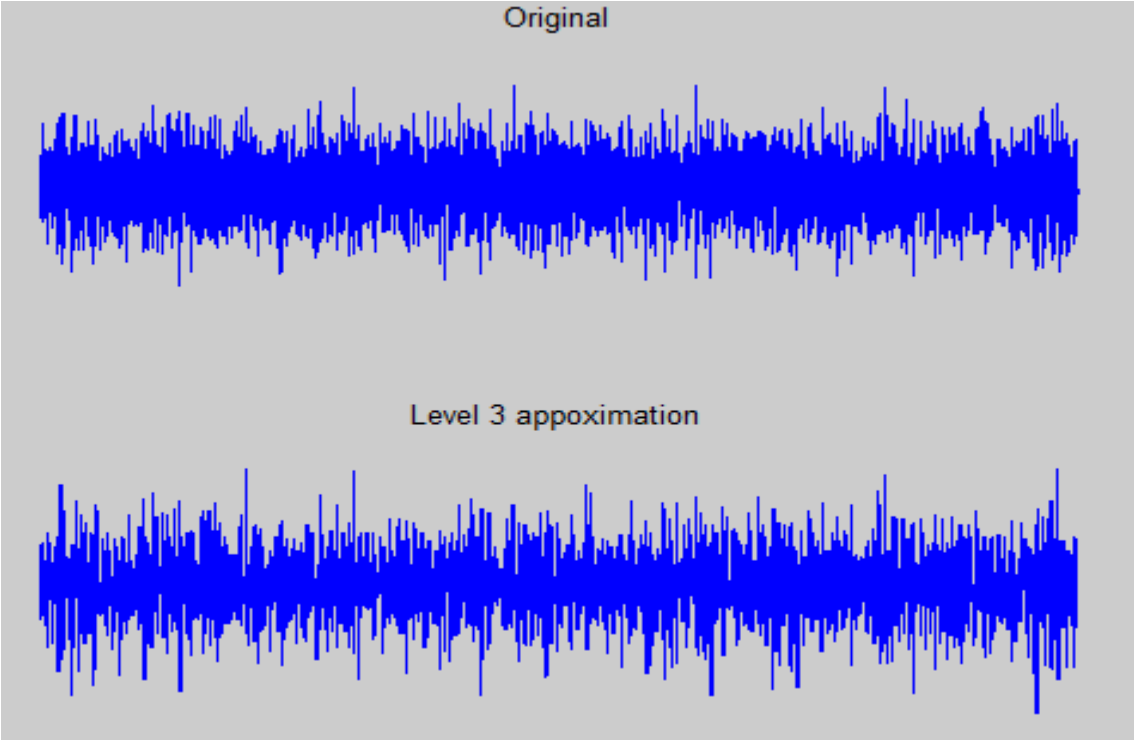

FIG_4.1(C) Original signal with level 3 approximation de-noise

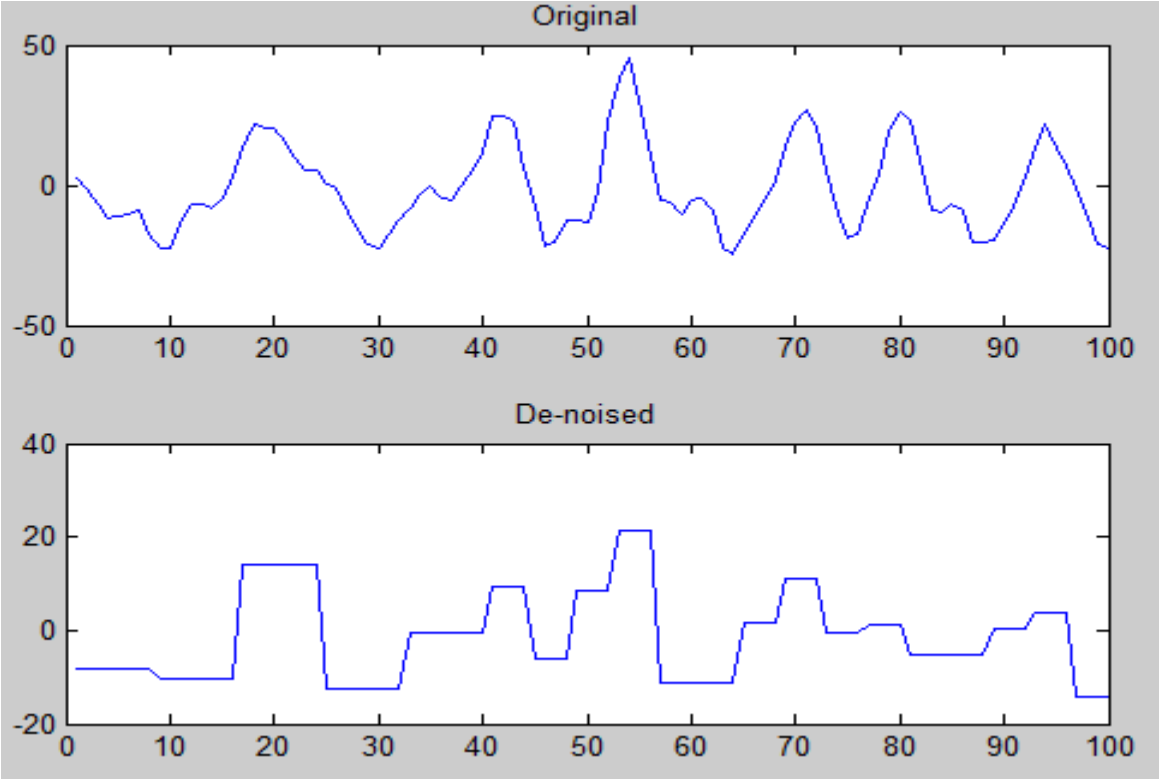

FIG_4.1(D) De-noised original signal

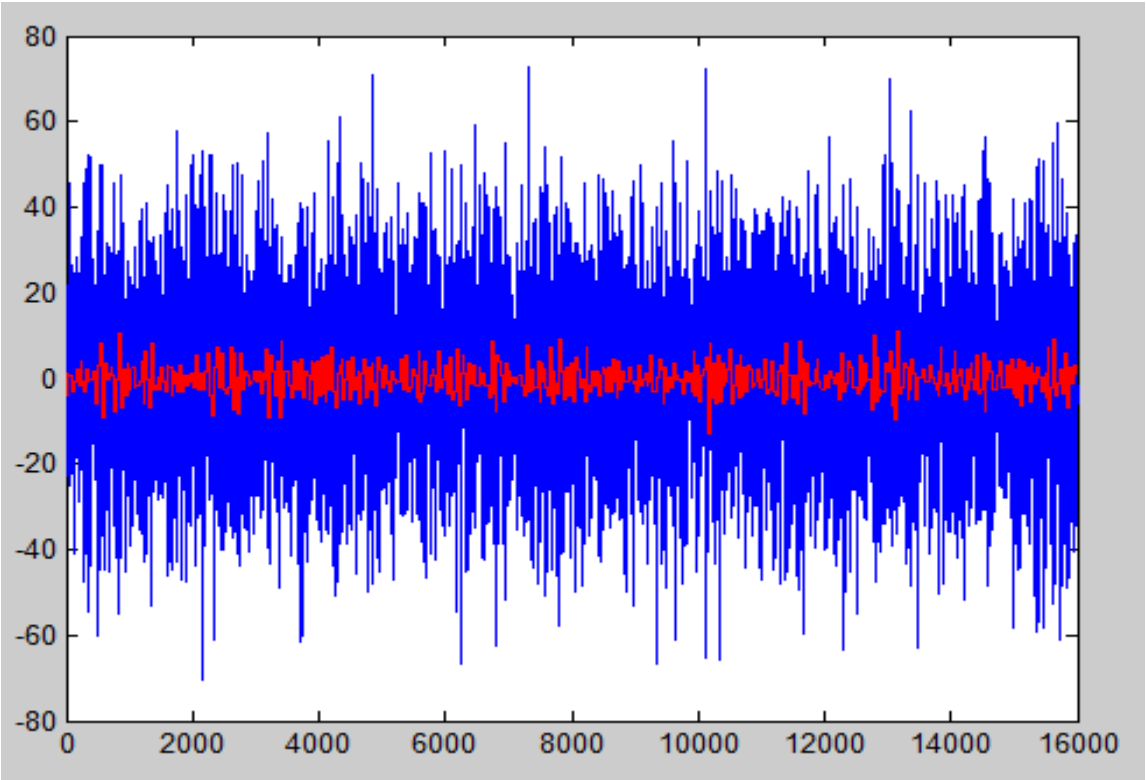

FIG_4.1(E) De-noised signal with original signal

Data : **r3hz_p53amp.txt**

We got the result of denoising the data of 3Hz oscillation as follows

ans = 75.5978

ans = 73.0846

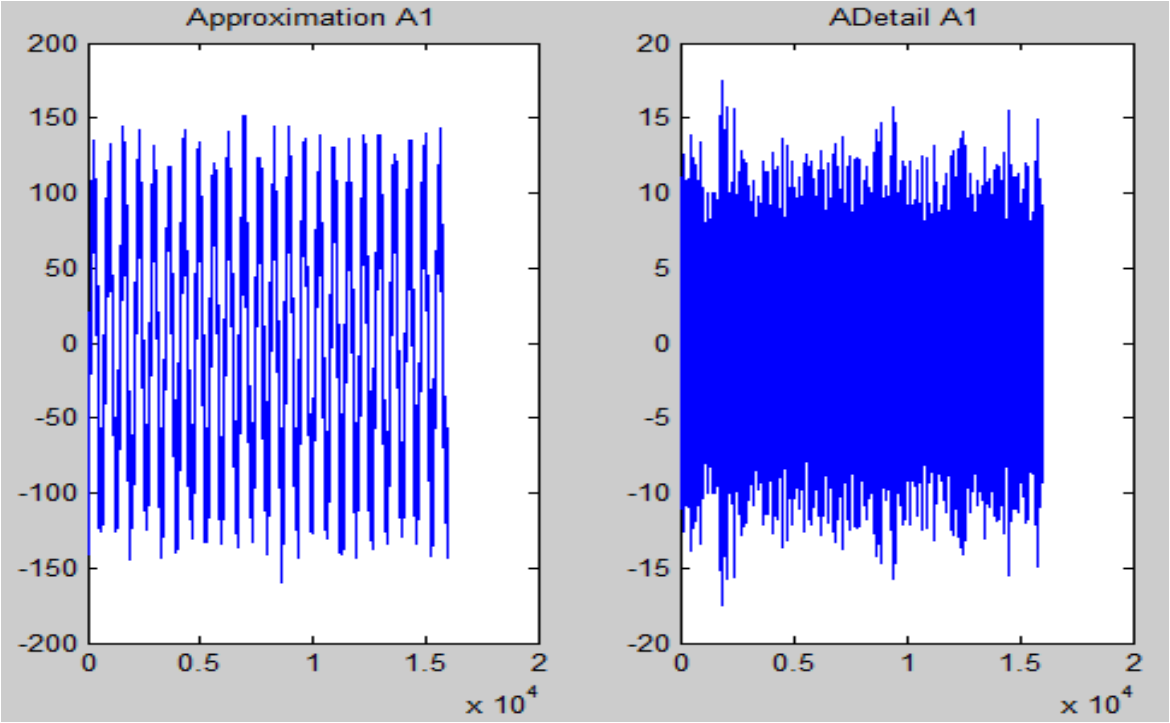

FIG_4.2(A) Approximation Haar de-noising

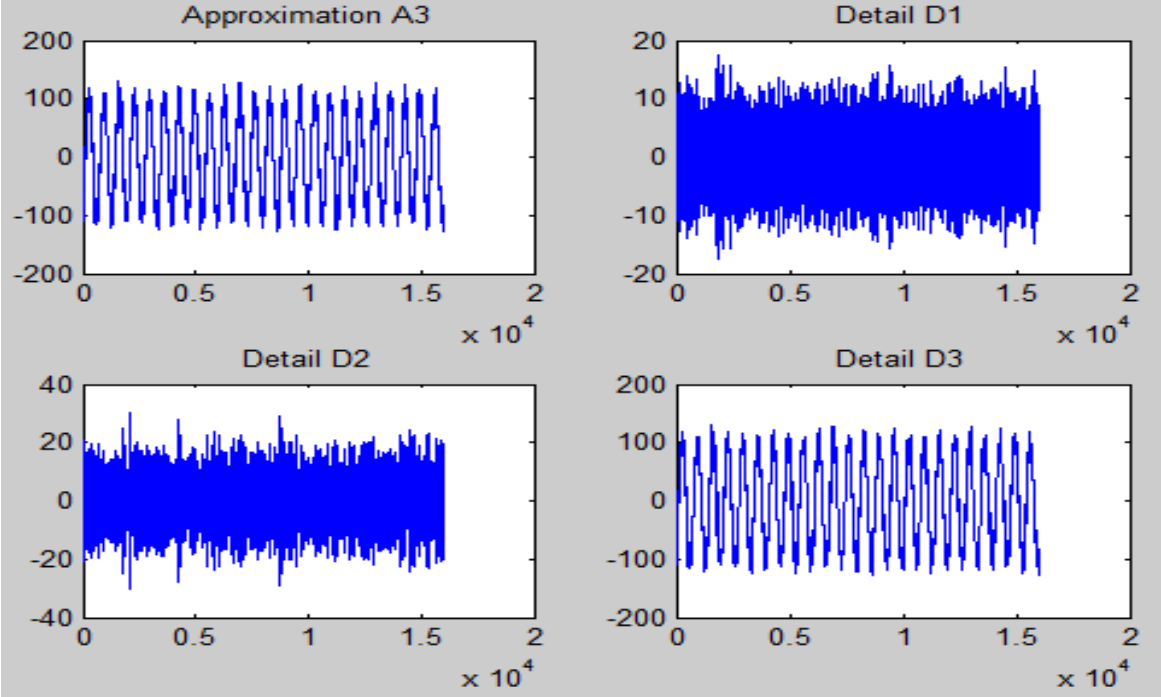

FIG_4.2(B) Approximation level 3 of Haar de-noising

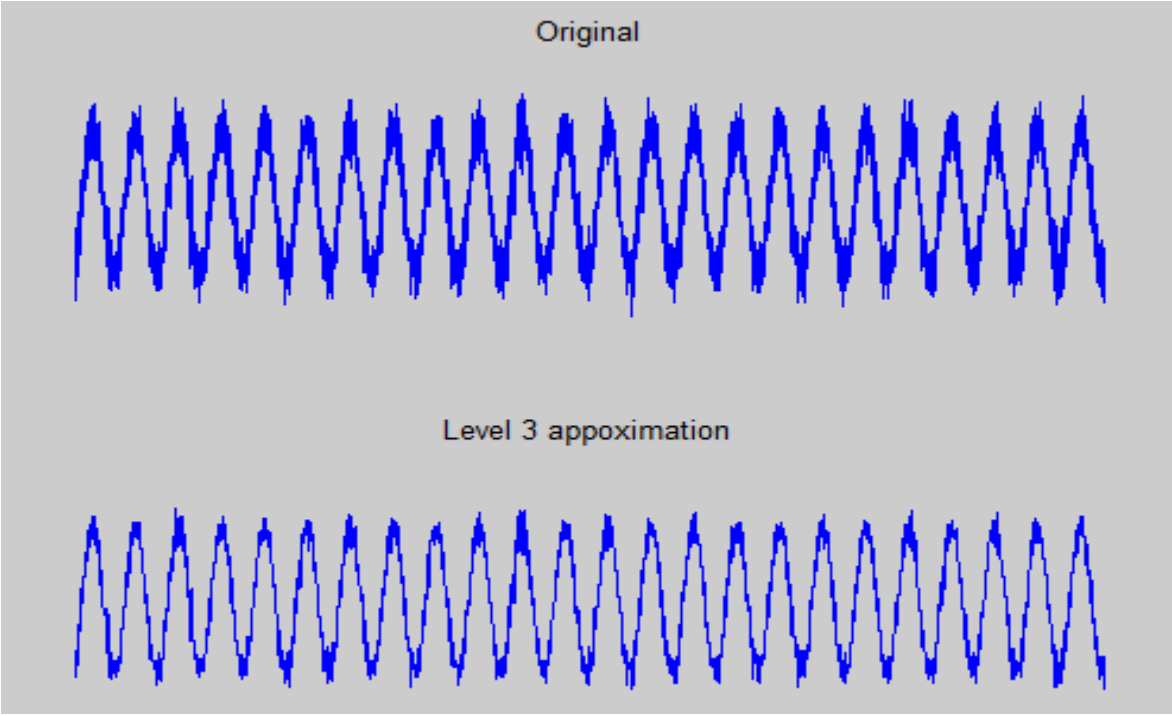

FIG_4.2(C) Original signal with level 3 approximation de-noise

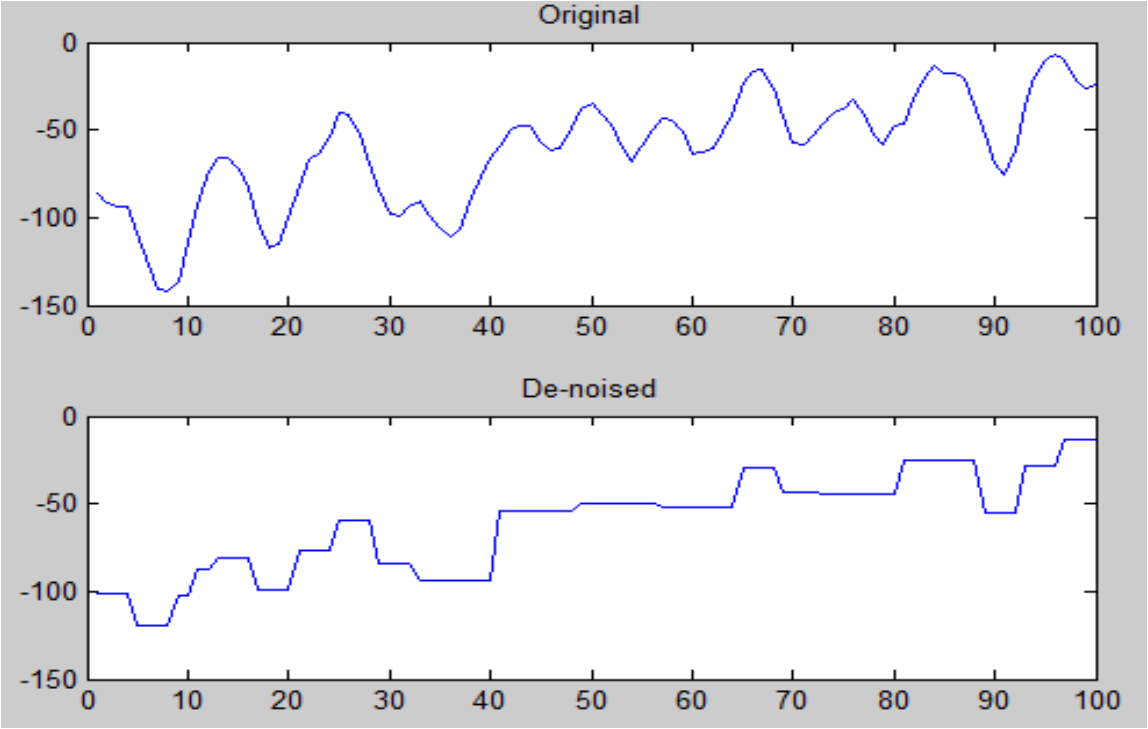

FIG_4.2(D) De-noised original signal

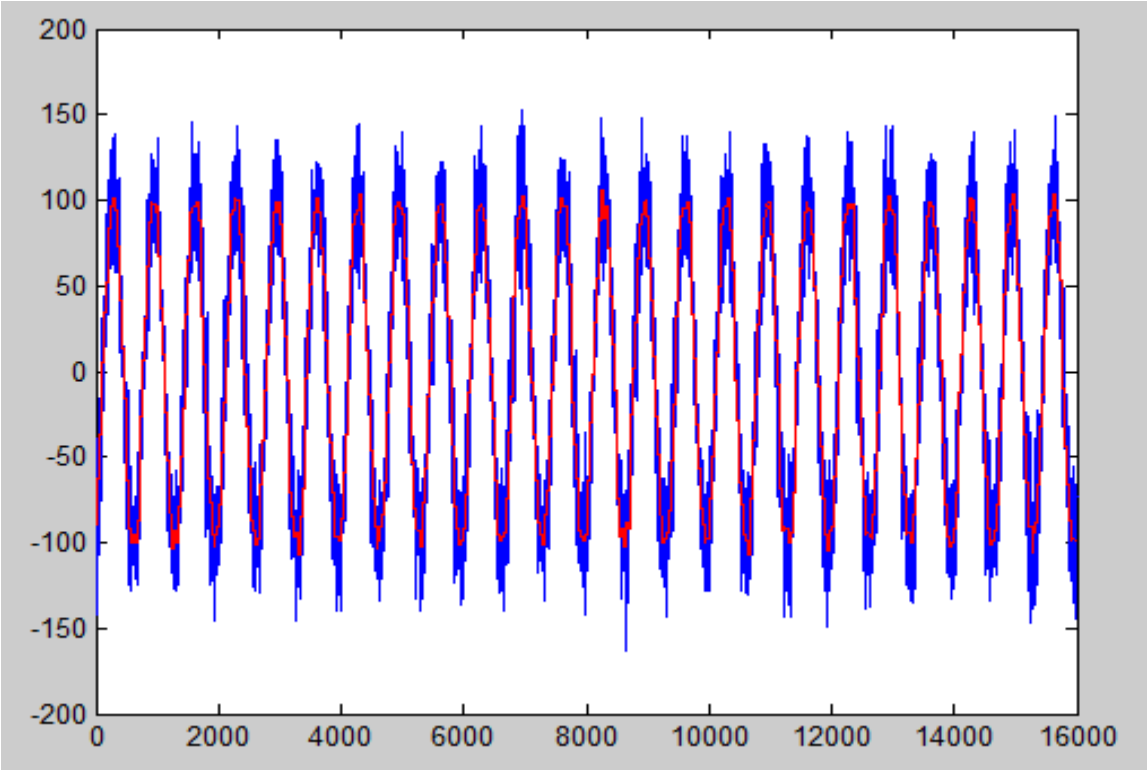

FIG_4.2(E) De-noised signal with original signal

DATA: **r10hz_p16amp.txt**

Original GyroData when the vehicle is in 10hz oscillation

We got the result by de-noising of data of 10 Hz oscillation as follows
ans =188.2850
ans = 79.6714

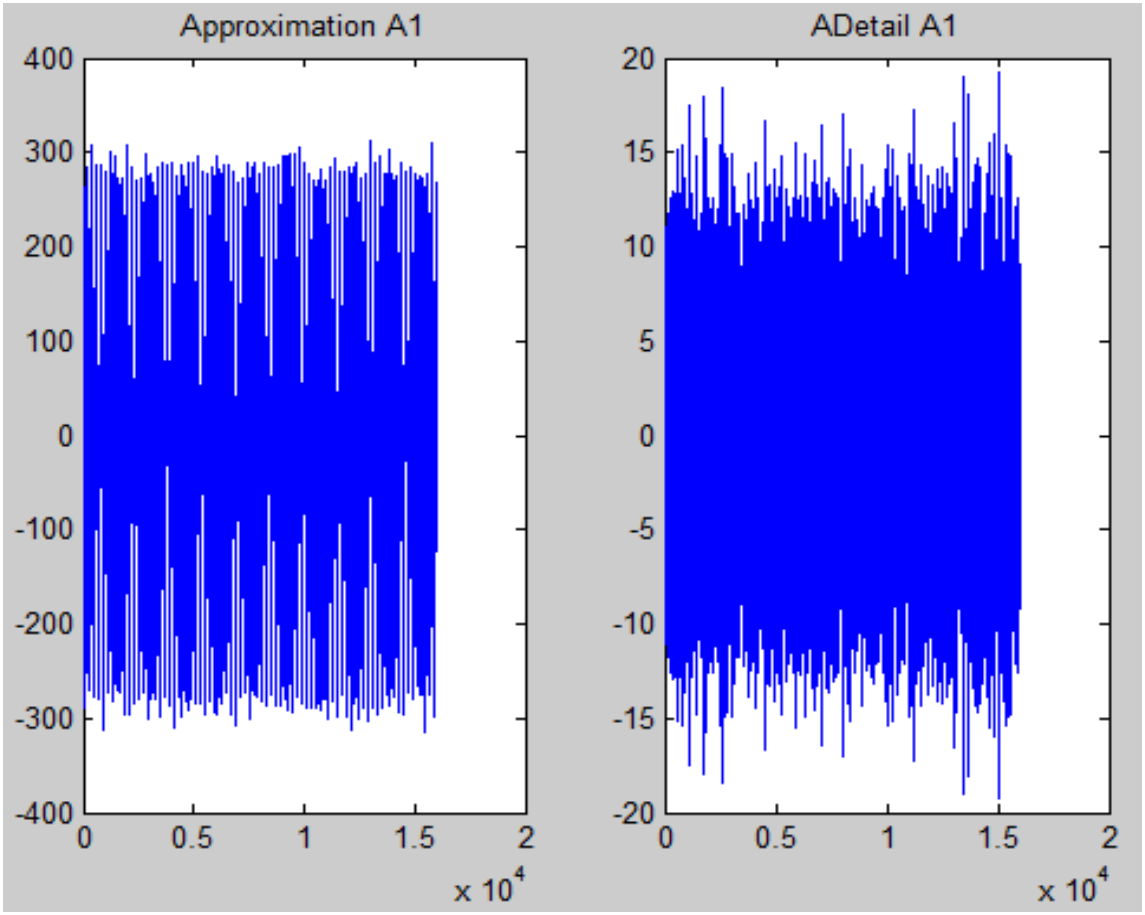

FIG_4.3(A) Approximation Haar de-noising

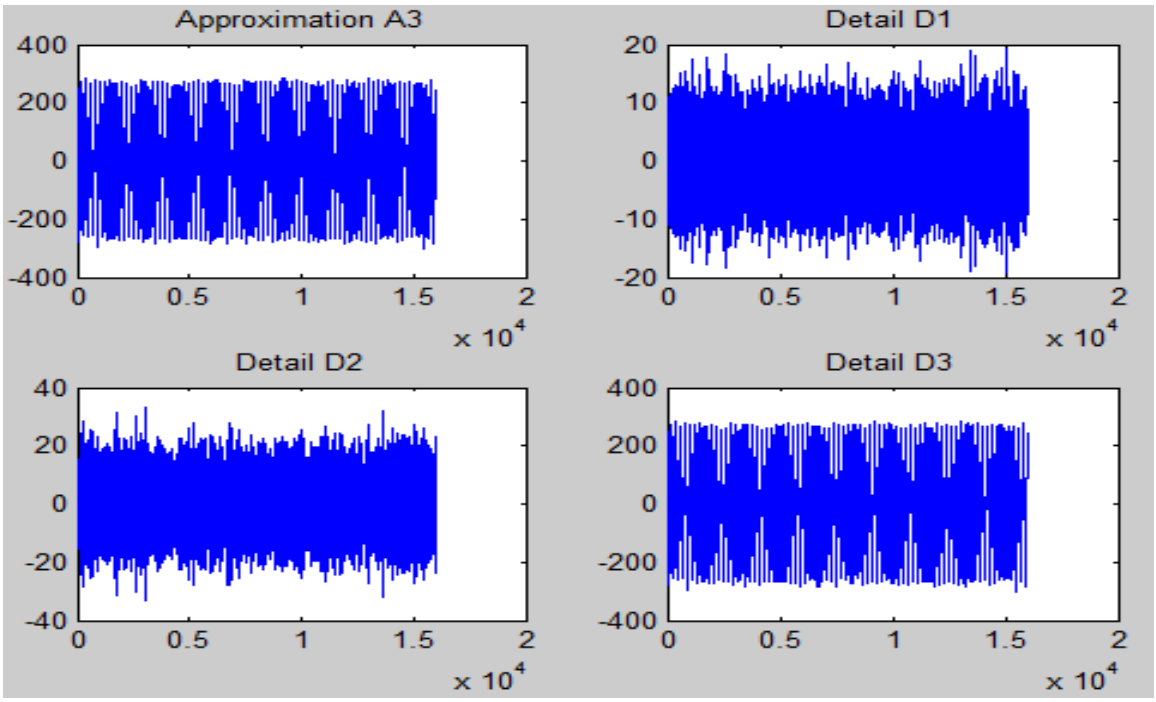

FIG_4.3(B) Approximation level 3 of Haar de-noising

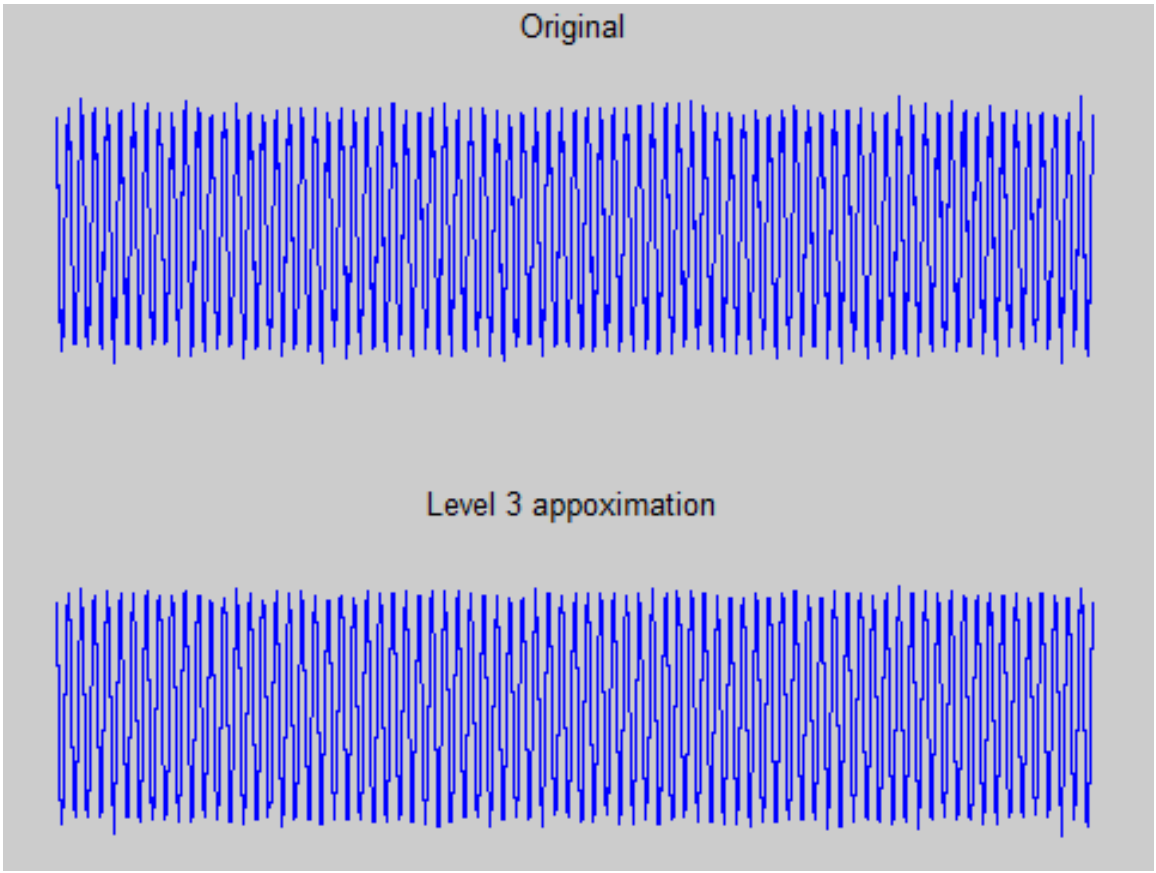

FIG_4.3(C) Original signal with level 3 approximation de-noise

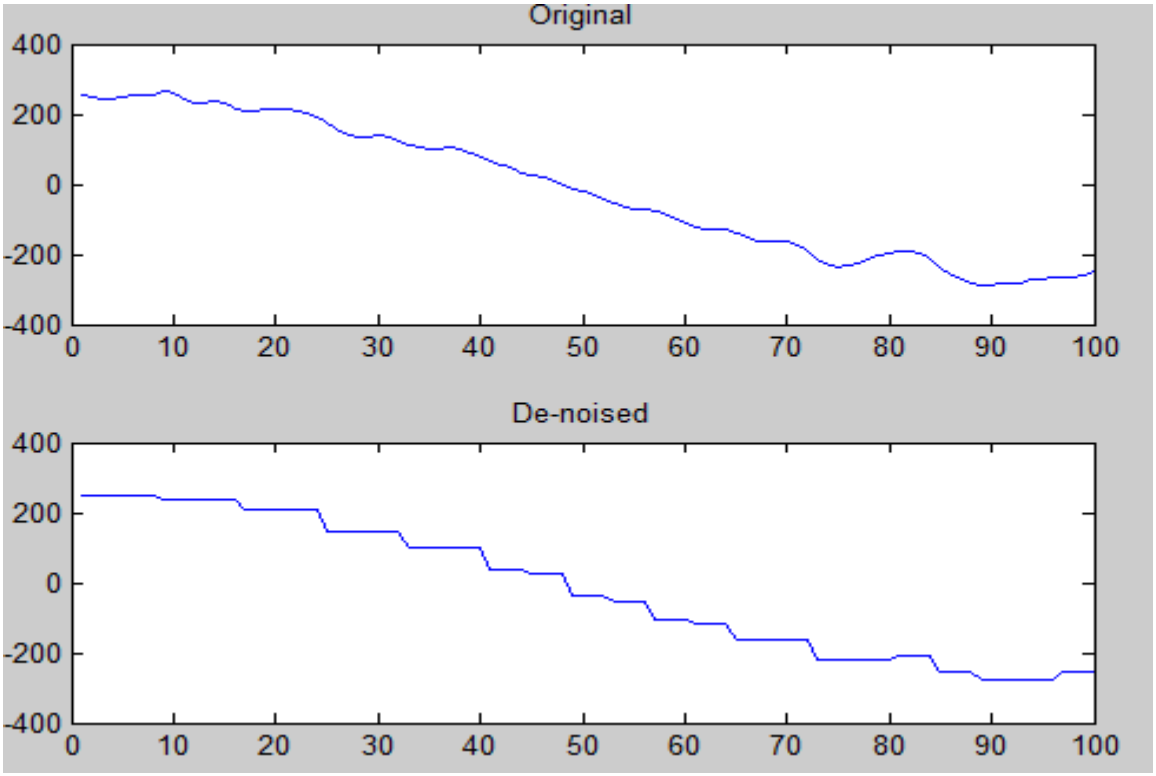

FIG_4.3(D) De-noised original signal

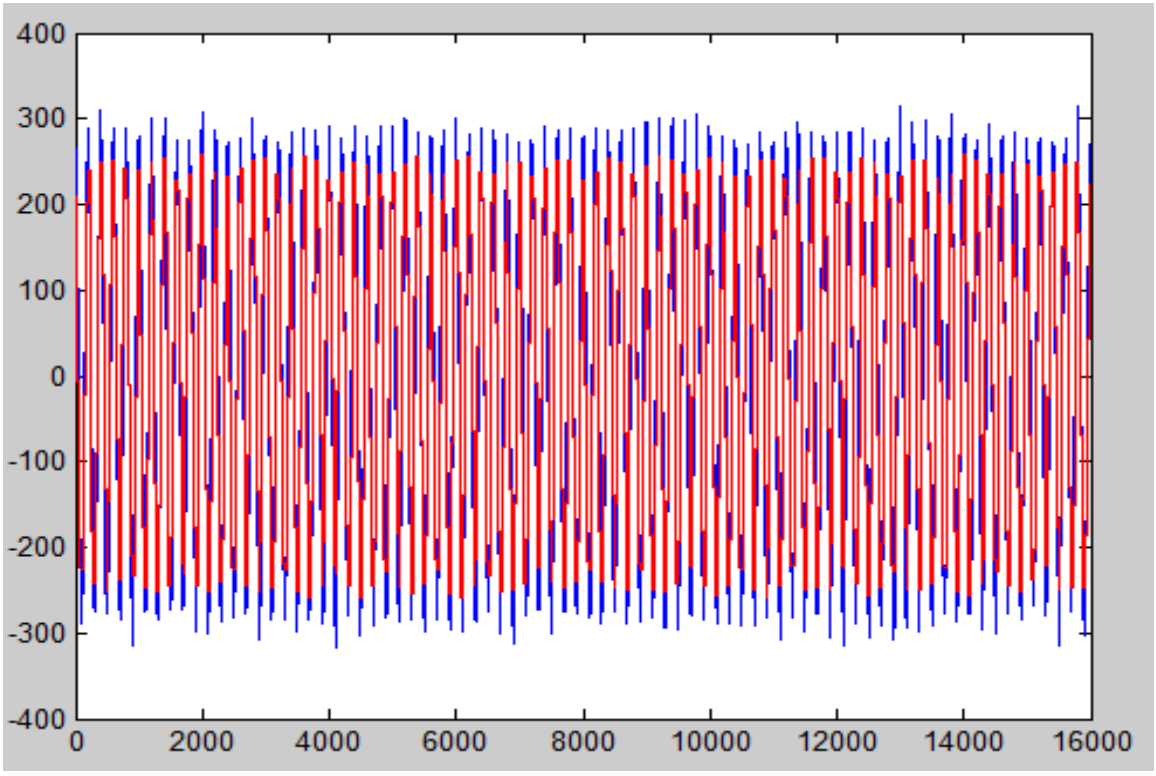

FIG_4.3(E) De-noised signal with original signal

DATA: **static2.txt**

Result of de-noising of data when vehicle is static using level 3 approximation

ans =18.7532 (BEFORE)

ans = 3.1215 (AFTER)

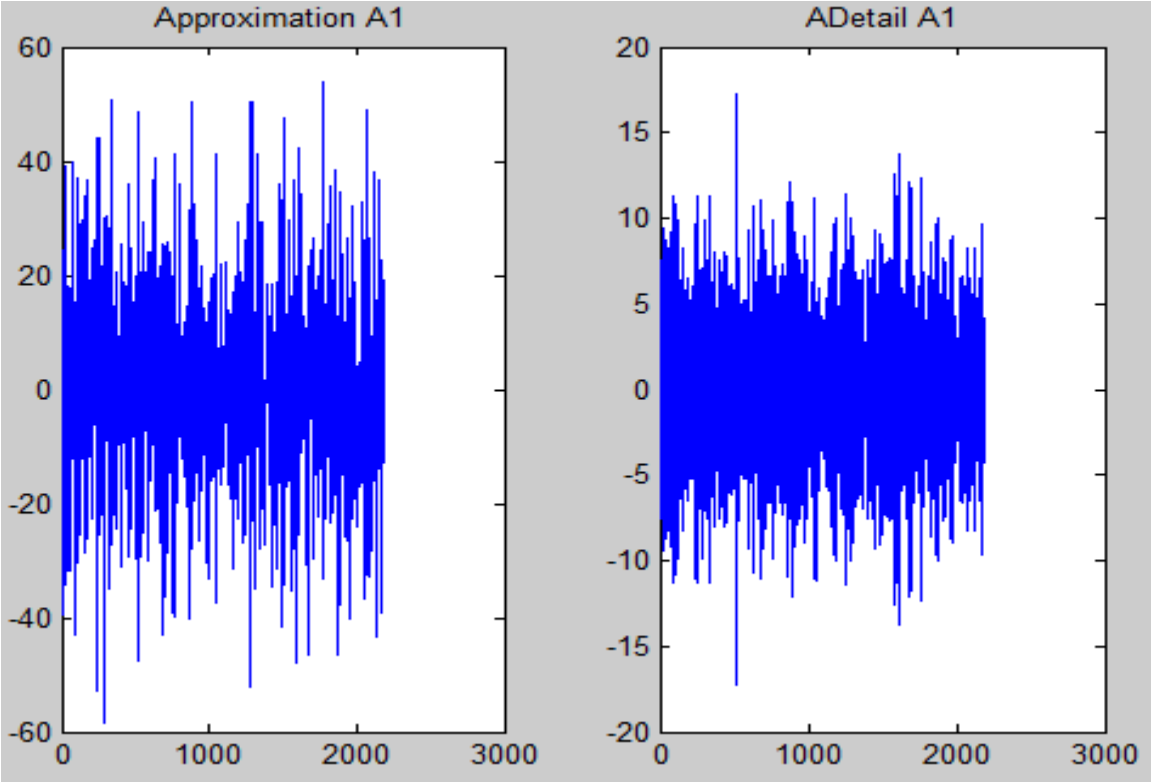

FIG_4.4(A) Approximation Haar de-noising

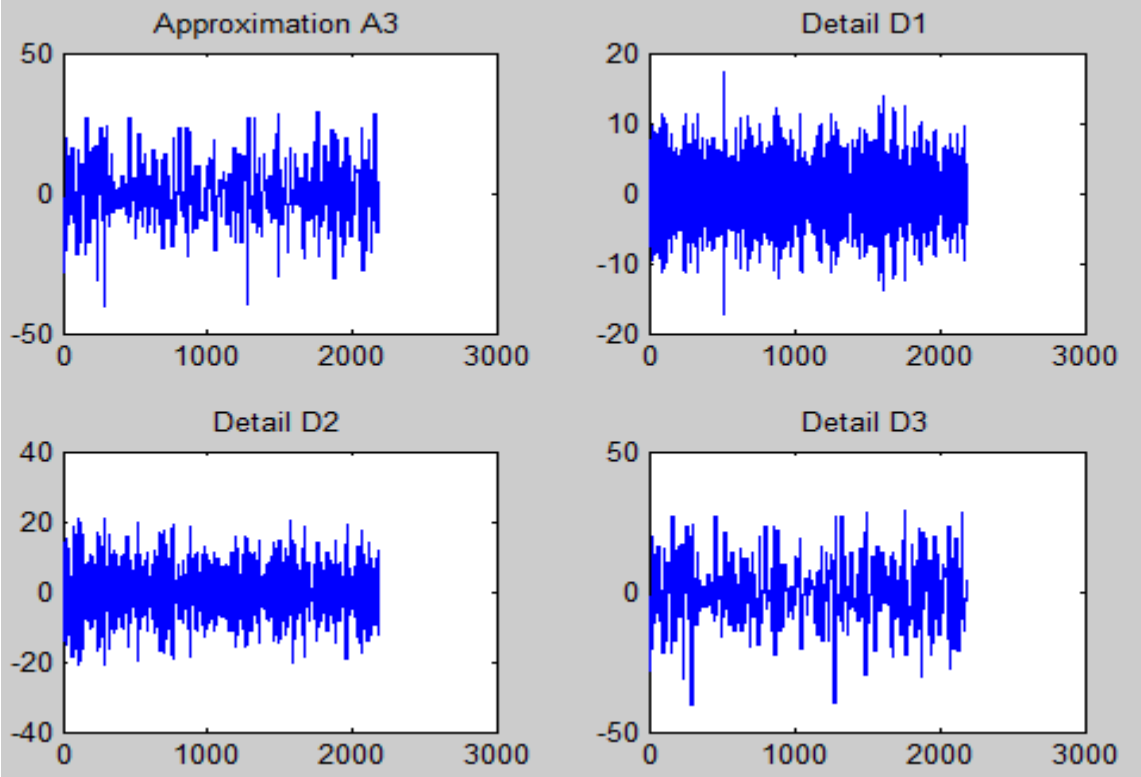

FIG 4.4(B) Approximation level 3 of Haar de-noising

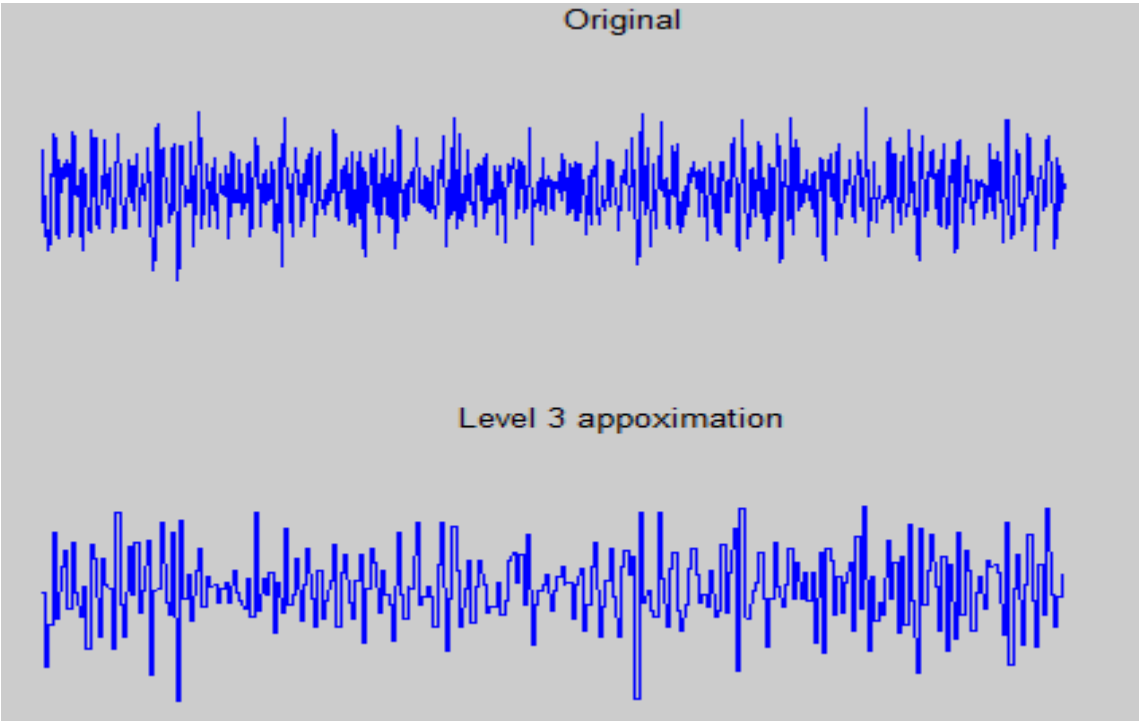

FIG_4.4(C) Original signal with level 3 approximation de-noise

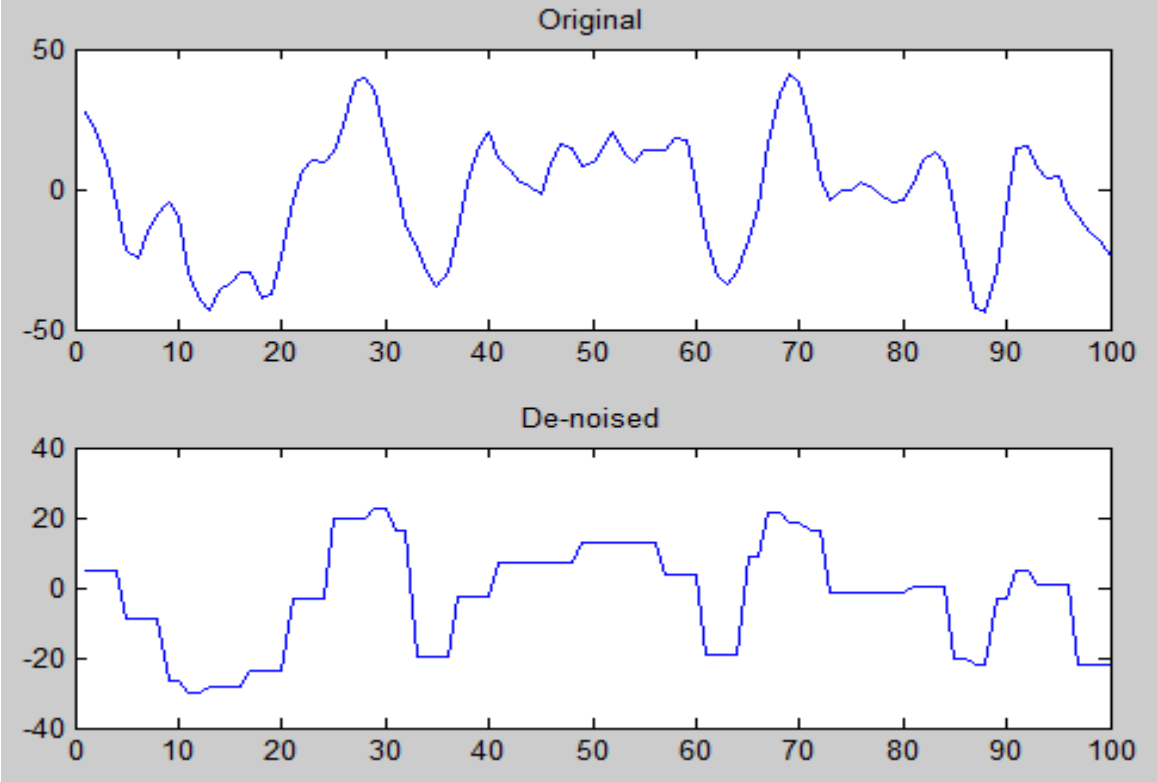

FIG_4.4(D) De-noised original signal

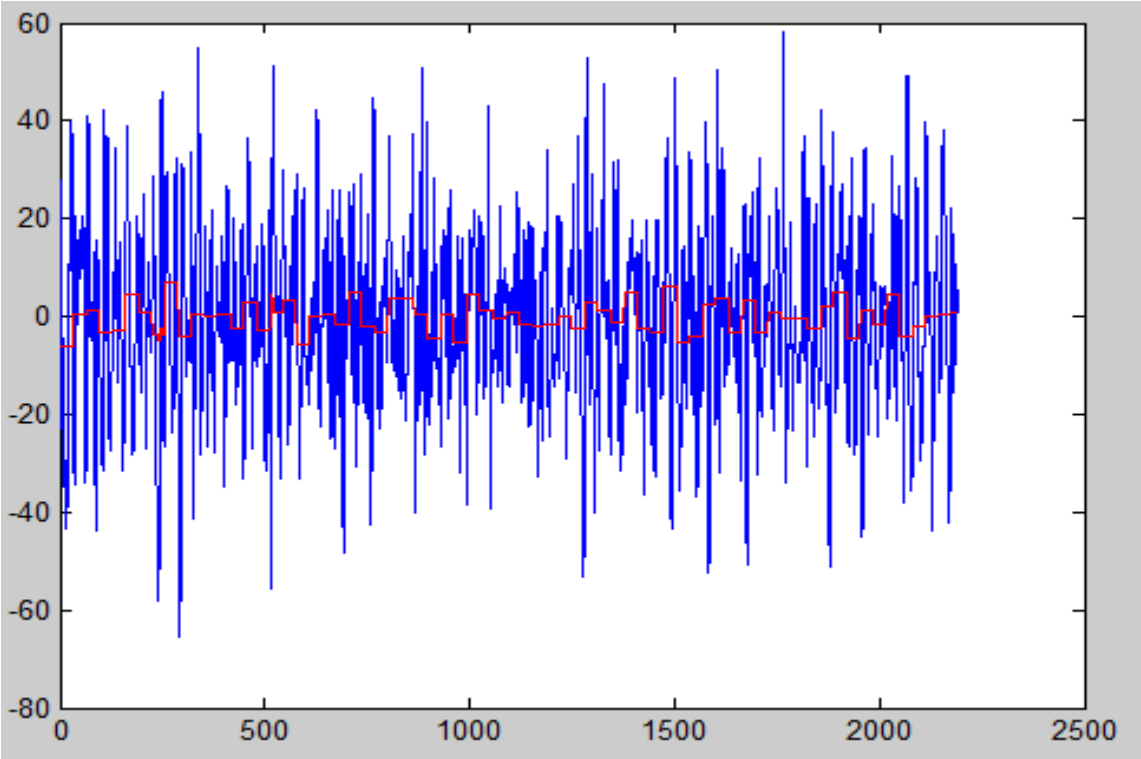

FIG_4.4(E) De-noised signal with original signal

DATA: **r10d_rate_run1.txt**

We got the result of de-noising of data when vehicle is 10 degree moving as follows

ans =19.0296
ans =3.6794

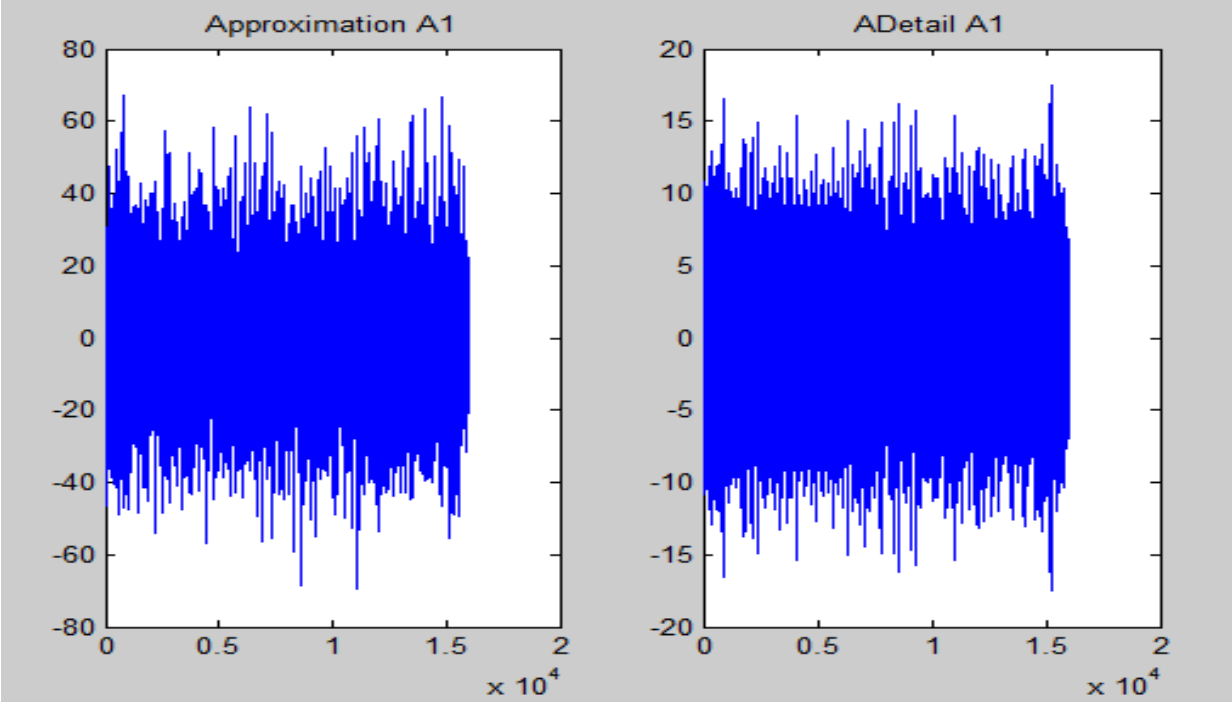

FIG_4.5(A) Approximation Haar de-noising

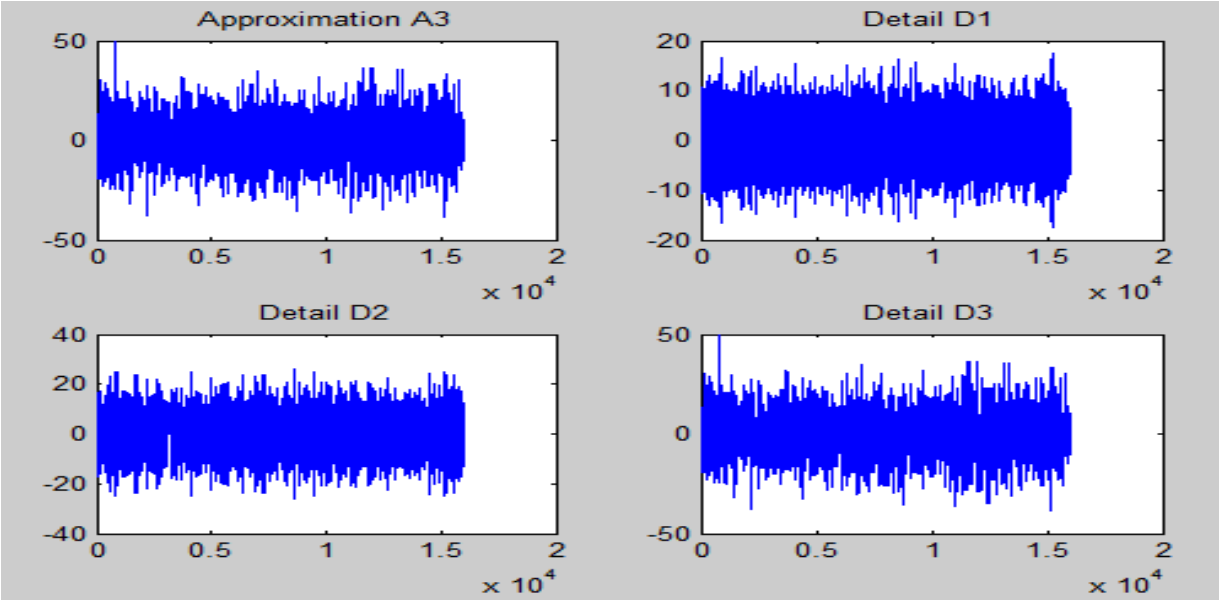

FIG_4.5(B) Approximation level 3 of Haar de-noising

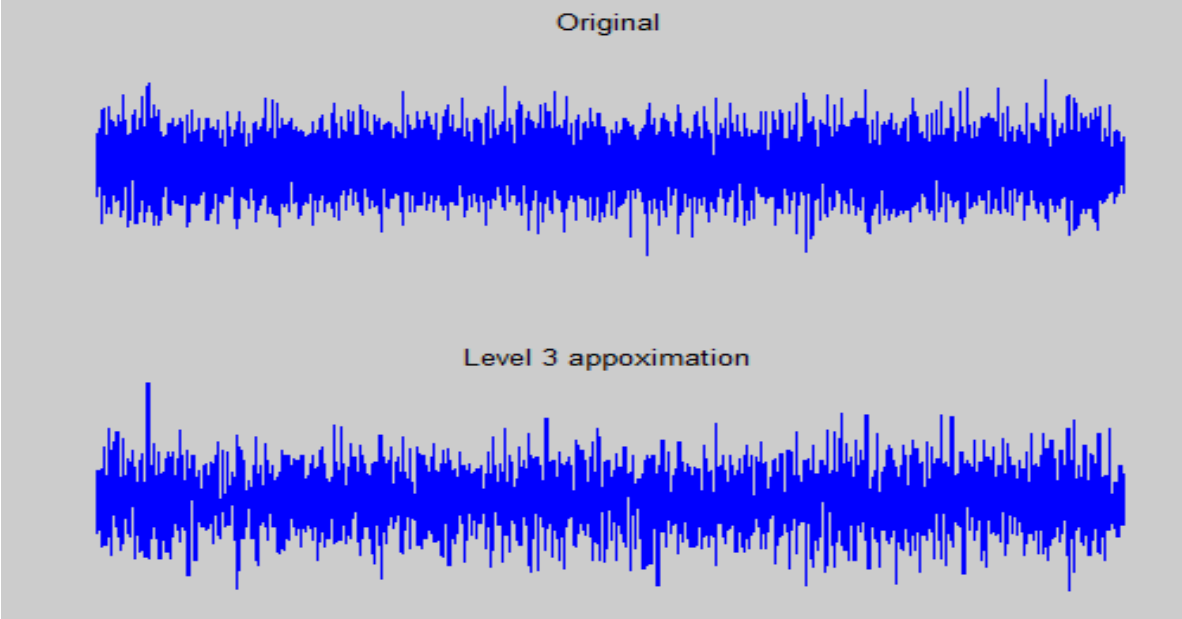

FIG_4.5(C) Original signal with level 3 approximation de-noise

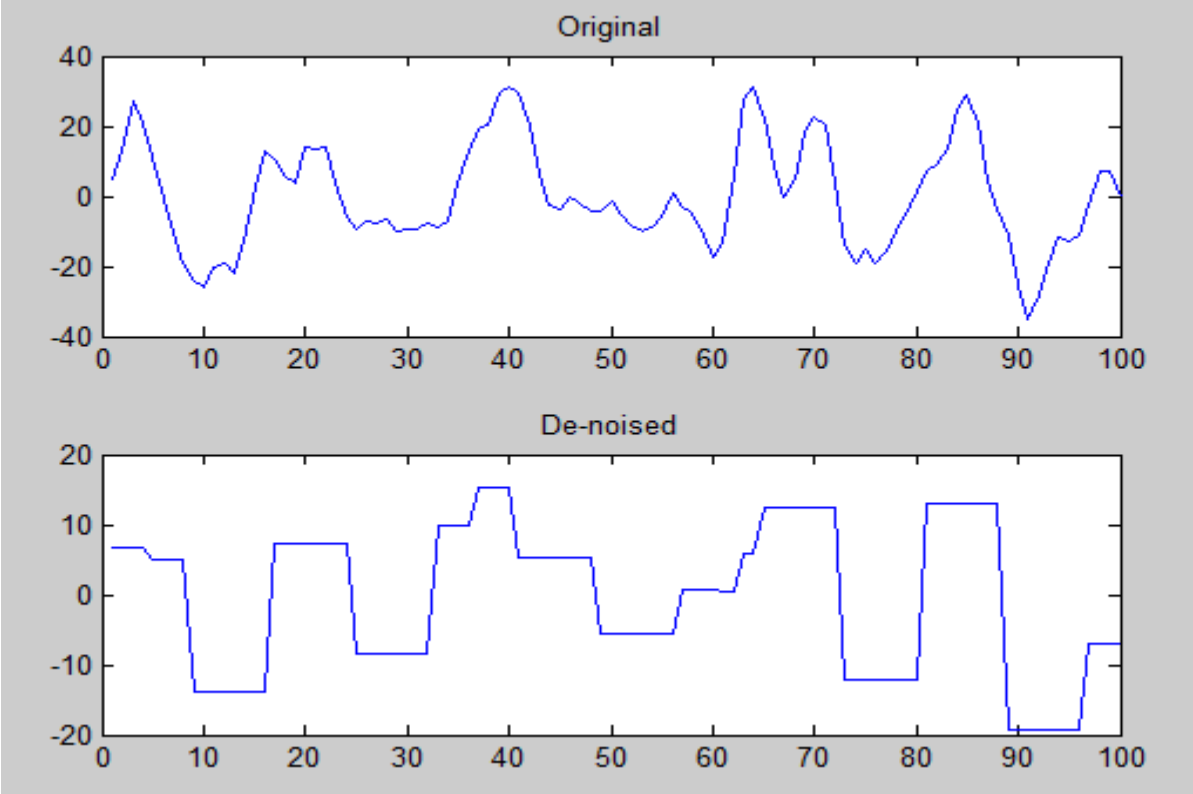

FIG_4.5(D) De-noised original signal

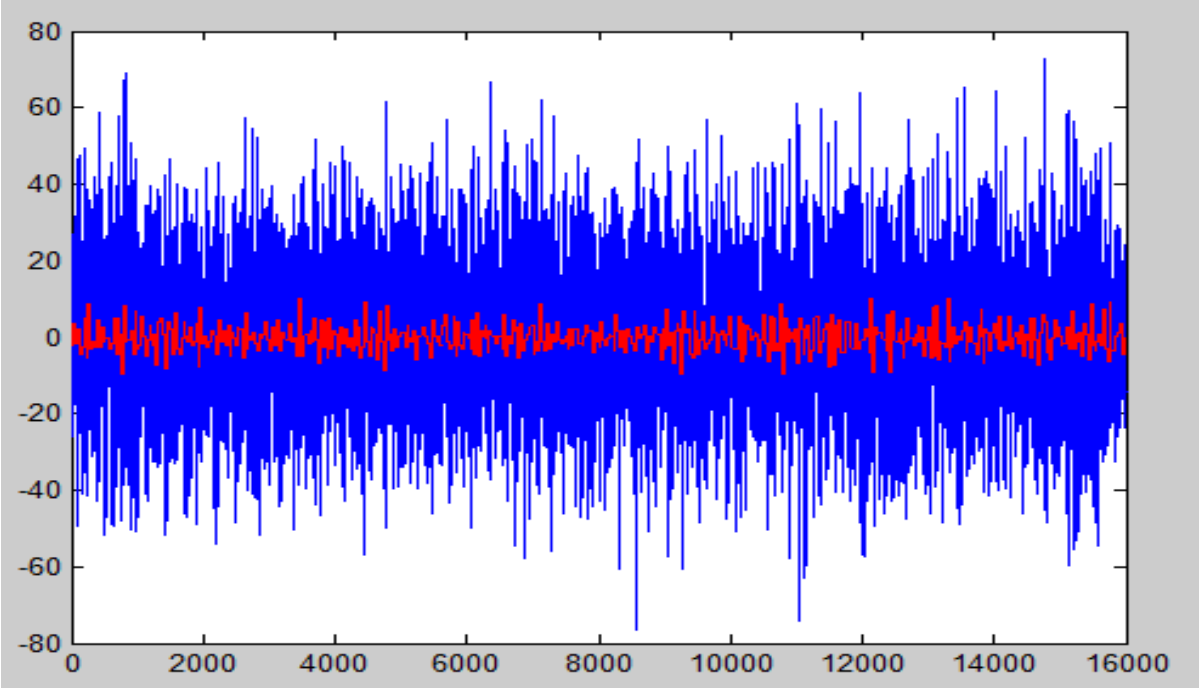

FIG_4.5(E) De-noised signal with original signal

DATA: **static1.txt**

We got the result of de-noising the data as follows

ans =17.8762

ans = 3.4568

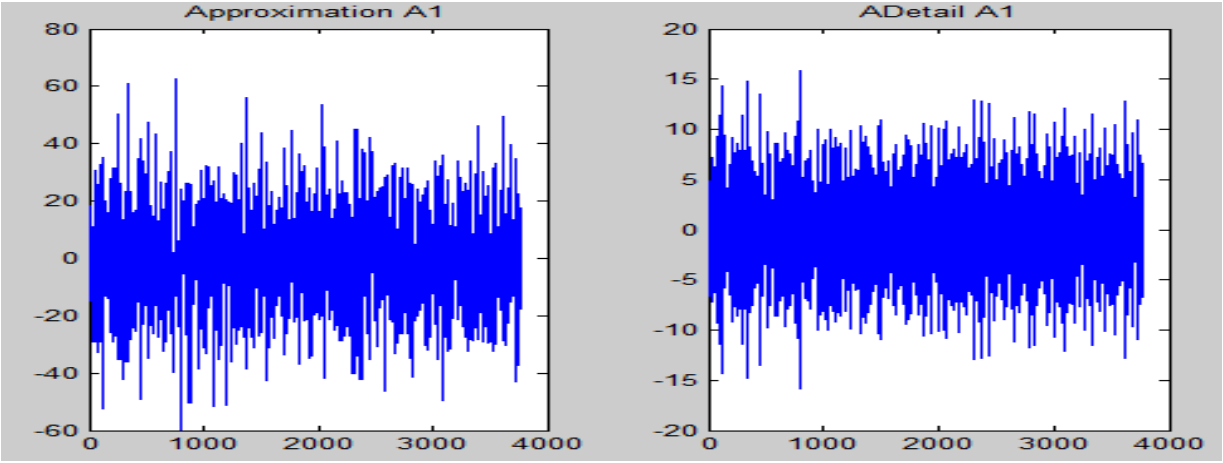

FIG 4.6(A) Approximation Haar de-noising

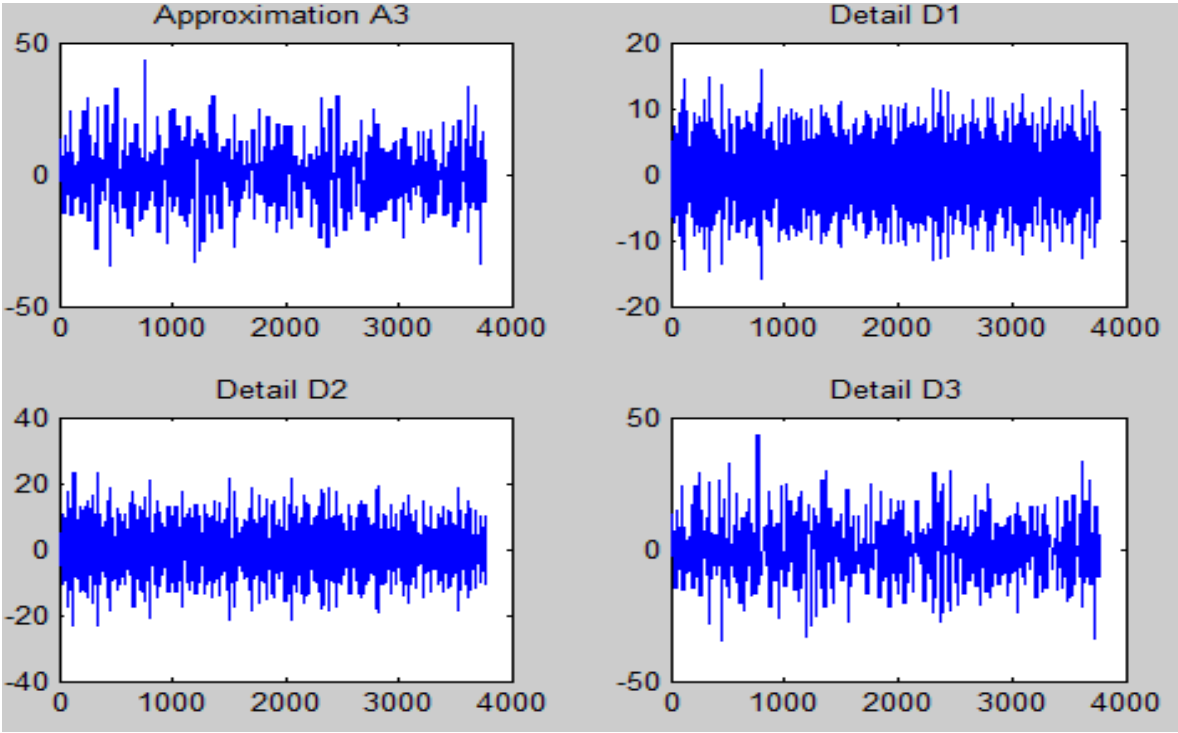

FIG_4.6(B) Approximation level 3 of Haar de-noising

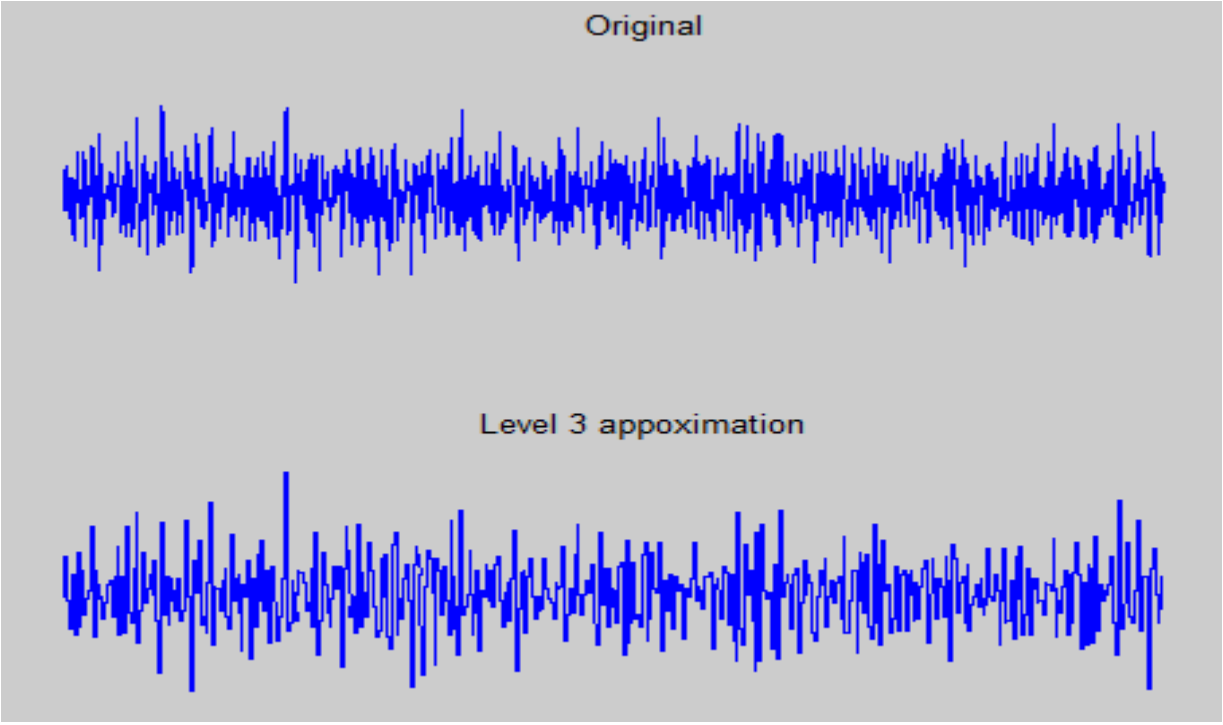

FIG_4.6(C) Original signal with level 3 approximation de-noise

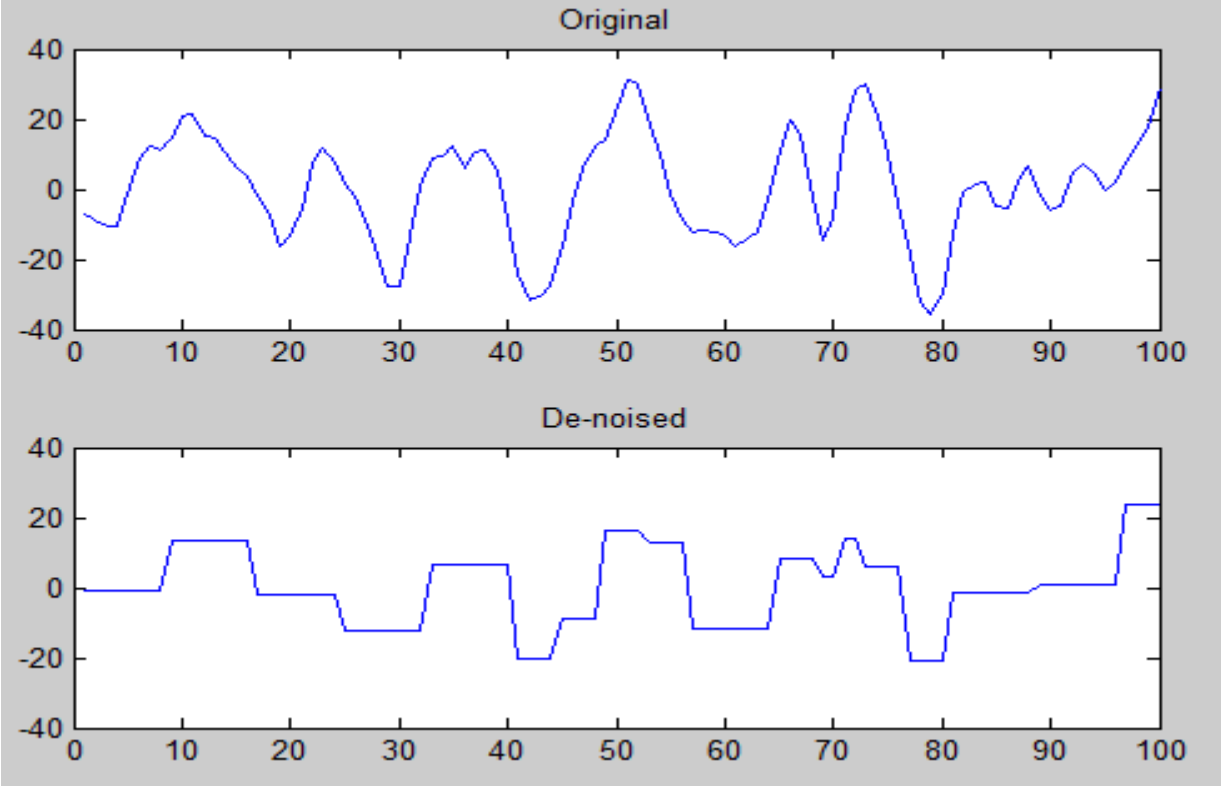

FIG_4.6(D) De-noised original signal

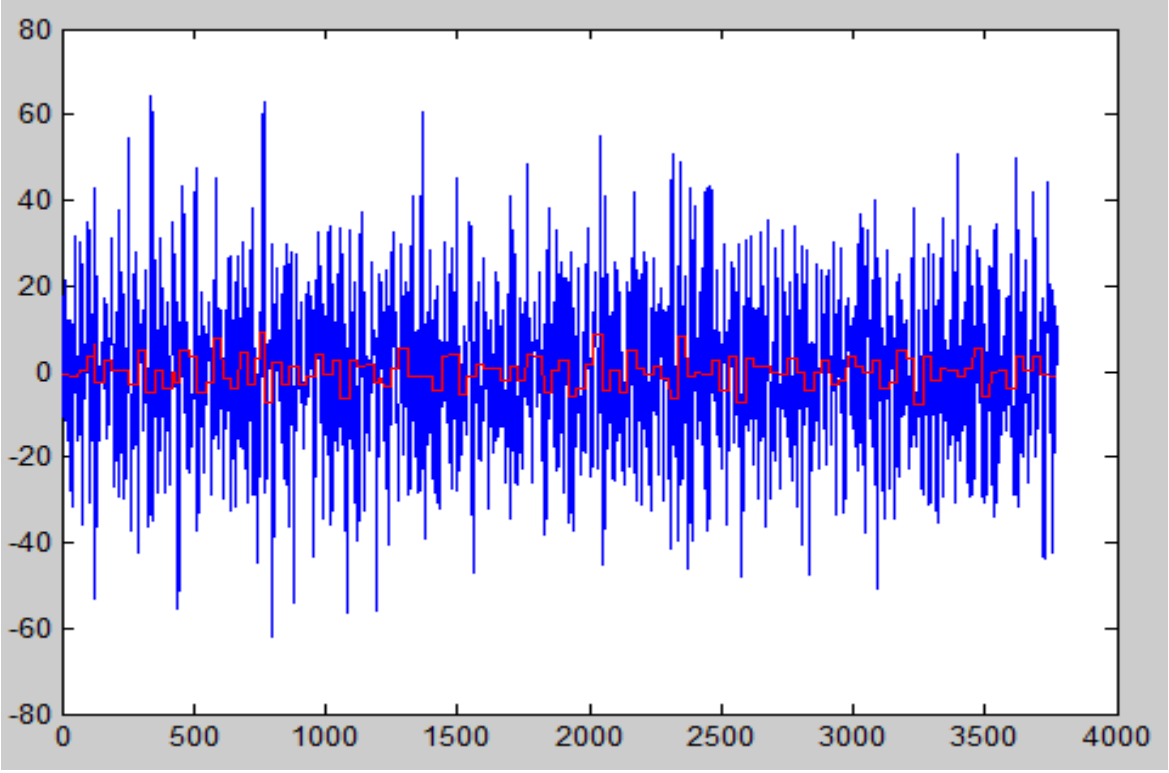

FIG_4.6(E) De-noised signal with original signal.

4.2 IMPLEMENTATION:

The algorithms developed in this thesis work can be implemented in real time using various techniques. One suggested methodology used dedicated digital signal processors to implement the logic. Following is the block diagram for implementation of the wavelet filter. In actual practice there are three MEMS gyros mounted in three orthogonal axes (X, Y, Z) on a cuboid and this is being interfaced to signal processing card.

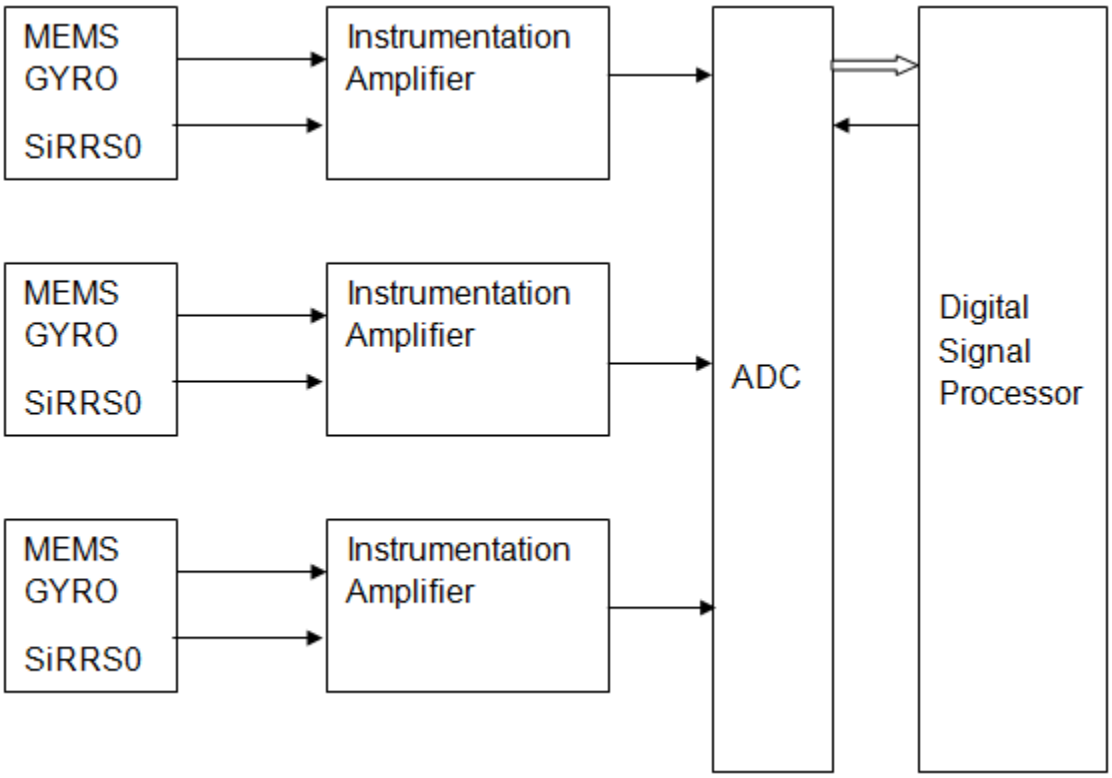

FIG 4.7 Implementation of MEMS gyro

4.2.1 General Description Of Instrumentation Amplifier:

Features

- Easy To Use
- Gain Set with One External Resistor (Gain Range 1 to 10000)
- Wide Power Supply Range (±2.3V to ±18V)
- Higher Performance than Three Op Amp IA Design
- Low Power 1.3mA max Supply Current
- Excellent DC Performance ("B Grade")
- 50 µV max, Input Offset Voltage
- 0.6µV/°C max, Input Offset Drift
- 1.0 nA max, Input Bias Current
- 100 dB min Common-Mode Rejection Ratio (G=10)
- Low Noise
- 9 nV/sqrHz, @ 1kHz, Input Voltage Noise
- 0.28 µV p-p Noise (0.1Hz to 10 Hz)
- Excellent AC Specifications
- 120 kHz Bandwidth (G=100)
- 15 µs Settling Time to 0.01%

Applications

- Weight Scales
- ECG and Medical Instrumentation
- Transducer Interface
- Data Acquisition Systems
- Industrial Process Controls
- Battery Powered and Portable Equipment

4.2.2. GENERAL DESCRIPTION OF ADC:

The system input is an acoustic sensor that drives a signal conditioning circuit which in turn drives an A/D converter. The sigma-delta converter was chosen because it contains a programmable gain front-end stage that can replace the signal conditioning circuit. Further, the sigma-delta ADC's fourth-order oversampling architecture provides signal-to-noise gain by moving the quantization noise up in frequency, where it is filtered out. This is a performance level that cannot be met by pipeline or successive-approximation architectures.

An ideal sensing system has the characteristics of good signal-to-noise ratio, low power consumption (for remote operation), programmable signal filtering to accommodate several applications, a variable sampling rate, and cost-effectiveness. An additional goal is to make the system easy to prototype for fast evaluation.

GENERAL DESCRIPTION OF DIGITAL SIGNAL PROCESSOR:

The ADSP-2106x are 32-bit processors optimized which are high performance DSP applications for Communications, Graphics, and Imaging Applications. The ADSP-2106x builds on the ADSP-21000 DSP core to form a complete system-on-a-chip, adding a dual-ported on-chip SRAM and integrated I/O peripherals supported by a dedicated I/O bus.

Fabricated in a high speed, low power CMOS process, the ADSP-2106x has a 25 ns instruction cycle time and operates at 40 MIPS. With its on-chip instruction cache, the processor can execute every instruction in a single cycle. The ADSP-2106x SHARC represents a new standard of integration for signal computers, combining a high performance floating-point DSP core with integrated, on-chip system features including a 4 Mbit SRAM memory host processor interface, DMA controller, serial ports, and link port and parallel bus connectivity for glue-less DSP multiprocessing.

The ADSP-2106x, illustrating the following architectural features:

- Computation Units (ALU, Multiplier and Shifter) with a
- Shared Data Register File
- Data Address Generators
- Program Sequencer with Instruction Cache
- Interval Timer
- On-Chip SRAM
- External Port for Interfacing to Off-Chip Memory and Peripherals
- Host Port and Multiprocessor Interface
- DMA Controller
- Serial Ports and Link Ports
- JTAG Test Access Port

4.3 CONCLUSION & FUTURE SCOPE OF WORK:

The experimental results are encouraging. We have to implement other wave function to see the performance, after that, we shall be in a position to choose the appropriate wavelet function for this particular application.

Using multilevel wavelet filter to achieve higher accuracy. This approach improves spike signal-to-noise ratio (SNR) and increases cluster discrimination. Additionally, the described technique is fast enough to be applied real-time.

In choosing a wavelet order, there is a tradeoff between SNR for initial detection and subsequent clustering performance. Although a higher wavelet filter has the most balanced performance, at some computational cost one could obtain even better results. Our results also show among IIR filters, using a Bessel filter is a far better option than regular Butterworth filtering.

Wavelet technique can be utilized to model the Gyro error and predict behavior a priory , so that corrective action can be taken out.

The developed wavelet denoising technique can be applied to MEMS accelerometer to improve it’s accuracy.

4.4 References:

1. V. Herrero, J. Cerdà, R. Gadea, M. Martínez, A. Sebastià " wavelet transform for INU system" proceedings of Group of Design of Digital Systems, Departamento de Ingeniería Electrónica. Universidad Politécnica de Valencia. Camino de Vera s/n, 46022 Valencia, SPAIN.
2. Ranran Yi, Bangcheng Han and Wei Sheng "Design on the Driving Mode of MEMS Vibratory Gyroscope"
3. Woon-Tahk Sung , Sangkyung Sung , Jang Gyu Lee and Taesam Kang "Design and performance test of a MEMS vibratory gyroscope with a novel AGC force rebalance control "
4. Steven Nasiri " A Critical Review of MEMS Gyroscopes Technology" 3150A Coronado Drive, Santa Clara, California 95054
5. Guofu Qu, Fan Zhao, Guizhong Liu, Hongzhao Liu " Adaptive MEMS Gyroscope Denoising Method Based on the à Trous Wavelet Transform"
6. Threshold Selection for Wavelet Shrinkage of Noisy Data by David L. Donoho and Iain M. Johnstone.
7. Application of Wavelet Packet Analysis in the De-noising of MEMS Vibrating Gyro by Wang Chang-hong, Huang Xu.
8. MEMS Gyro's Output Signal De-noising Based on Wavelet Analysis by Fuqiang Liu, Fanming Liu, Wenjing Wang and Bo Xu.
9. Filtering Research of MEMS Gyro Drift Signal Based on Local Wave Decomposition by Yuan Gannan, Yang Jingian.
10. Wavelets and Wavelet Transform by C. Sidney Burrus, Ramesh A. Gopinath.
11. Wavelets Made Easy by Yves Nievergelt.
12. The Wavelet Tutorial by Robi Polikar.
13. De-noising by Soft-Thresholding by David L. Donoho.
14. Insight into WAVELETS from Theory to Practice by K.P. Soman and K.I. Ramachandran.

15. “Research Of The Gyro Signal De-Noising Method Based On Stationary Wavelets Transform” by JICHANG GUO , JIANFU TENG
16. Calibration Of A Mems Inertial Measurement Unit by *Isaac Skog*, *Peter H¨Andel*2 Xvii Imeko World Congress
17. Wavelet Analysis And Its Applications by Gaoyou Tian and Wanzhen Lu
18. “MEMS Vibratory Gyroscopes A Structural Approaches to Improve Robustness” by Cenk Acar and Andrei Shkel
19. N. Yazdi, F. Ayazi, and K. Najafi. Micromachined Inertial Sensors. Proc. of IEEE, Vol. 86,No. 8, August 1998.
20. Hopkin, I. D. Vibrating gyroscopes (automotive sensors). IEEE Colloquium on Automative Sensors. Digest No. 1994/170. Solihull, UK, Sept. 1994,
21. Integrated Micro-electromechanical Gyroscopes by Huikai Xie and Gary K. Fedder

DOI: 10.1061/~ASCE!0893-1321~2003!16:2~65

22. T. K. Tang, R. C. Gutierrez, C. B. Stell, V. Vorperian, G. A. Arakaki, J. T. Rice, W. J. Li, I. Chakraborty, K. Shcheglov, J. Z. Wilcox, and W. J. Kaiser. A packaged silicon MEMS vibratory gyroscope for microspacecraft. Proc. IEEE Micro Electro Mechanical Systems Workshop (MEMS’97), Japan, 1997